Title 1: A CRMP4-Dependent Retrograde Axon-to-Soma Death Signal in Amyotrophic Lateral Sclerosis

Running Title: – Retrograde Axonal Death Signal in ALS

Authors:

Roy Maimon[1*], Lior Ankol[1,2*], Tal Gradus Pery[1], Topaz Altman[1], Ariel Ionescu[1], Romana Weissova[3,4], Michael Ostrovsky[1], Elizabeth Tank[5], Gayster Alexandra[7], Natalia Shelestovich[1,7], Yarden Opatowsky[8], Amir Dori[1,2,6], Sami Barmada[5], Martin Balastik[3], and Eran Perlson[1, 2#]

Affiliations:

[1]Sackler Faculty of Medicine, Tel Aviv University, Tel Aviv 69978, Israel

[2]Sagol School of Neuroscience, Tel Aviv University, Tel Aviv 69978, Israel

[3]Institue of Physiology of the Czech Academy of Sciences, Prague, Czech Republic

[4]Faculty of Science, Charles University, Prague, Czech Republic

[5]Department of Neurology, University of Michigan, Ann Arbor, Michigan USA

[6]Department of Neurology, Sheba Medical Center, Tel Hashomer, Ramat Gan, Israel

[7]Department of Pathology, Sheba Medical Center, Tel Hashomer, Ramat Gan, Israel

[8]The Mina and Everard Goodman Faculty of Life Science, Bar Ilan University, Israel

* Equally contributing authors

[#]Corresponding Author:

Eran Perlson, Ph.D., Dept. of Physiology and Pharmacology, Sackler Faculty of Medicine, Room 605, Sagol School of Neuroscience, Tel Aviv University, Ramat Aviv, Tel Aviv 69978, Israel. +972-3-6408743 eranpe@tauex.tau.ac.il

Key Words:

Retrograde Signaling, CRMP4, Axonal Transport, ALS, Dynein

Abstract

Amyotrophic Lateral Sclerosis (ALS) is a fatal non-cell-autonomous neurodegenerative disease characterized by the loss of motor neurons (MNs). Mutations in CRMP4 are associated with ALS in patients, and elevated levels of

CRMP4 are suggested to affect MN health in the SODG93A-ALS mouse model. However, the mechanism by which CRMP4 mediates toxicity in ALS MNs is poorly understood. Here, by using tissue from human patients with sporadic ALS, MNs derived from C9orf72-mutant patients, and the SOD1G93A-ALS mouse model, we demonstrate that subcellular changes in CRMP4 levels promote MN loss in ALS. First, we show that while expression of CRMP4 protein is increased in cell bodies of ALS-affected MN, CRMP4 levels are decreased in the distal axons. Cellular mislocalization of CRMP4 is caused by increased interaction with the retrograde motor protein, dynein, which mediates CRMP4 transport from distal axons to the soma and thereby promotes MN loss. Blocking the CRMP4-dynein interaction reduces MN loss in human-derived MNs (C9orf72) and in ALS model mice. Thus, we demonstrate a novel CRMP4-dependent retrograde death signal that underlies MN loss in ALS.

Introduction

Amyotrophic lateral sclerosis (ALS) is a lethal neurodegenerative disease that is characterized by degeneration of upper and lower motor neurons (MN). This process leads to spasticity, muscle atrophy, and paralysis, which develop into respiratory failure and patient death (Peters *et al*, 2015; Fischer *et al*, 2004; Frey *et al*, 2000; Moloney *et al*, 2014; Boillée *et al*, 2006). The most common mutations responsible for familial ALS (fALS) include expansions of a repeated DNA element (GGGGCC) in the *C9orf72* gene, and point mutations in the superoxide dismutase 1 (SOD1) gene (Rosen *et al*, 1993; Renton *et al*, 2011; DeJesus-Hernandez *et al*, 2011).

A hallmark finding in ALS patients, as well as in ALS mouse models, is alterations in axonal transport (Perlson *et al*, 2010; De Vos & Hafezparast, 2017; Gershoni-Emek *et al*, 2015; Bilsland *et al*, 2010). In order to survive and function, MNs depend upon the propagation of signalling events along the axons between the synapse and soma (cell body) (Millecamps & Julien, 2013; Harrington & Ginty, 2013; Terenzio *et al*, 2017; Zahavi *et al*, 2017). Retrograde and anterograde axonal transport are mediated by the dynein/dynactin and kinesin motor protein families, respectively (Paschal & Vallee, 1987; Howard *et al*, 1989; Guedes-Dias & Holzbaur, 2019) .Notably, mutations in kinesin and dynein/dynactin are also associated with ALS in humans (LaMonte *et al*, 2002; Nicolas *et al*, 2018; Steinberg *et al*, 2015; Münch *et al*, 2004). Several studies have suggested that alterations in cross-talk and long-distance signaling pathways between neurons and their diverse extracellular

cues, which are mediated by axonal transport, contribute to ALS pathology (Perlson *et al*, 2009; Gibbs *et al*, 2018; Boillée *et al*, 2006).

Collapsin Response Mediator Proteins (CRMPs) constitute a family of developmentally-regulated phosphoproteins known for their intracellular mediation of class 3 Semaphorin signaling (Goshima *et al*, 1995; Ziak *et al*, 2020). There are 5 known CRMPs in vertebrates, all of which share ~75 percent sequence similarities (Schmidt & Strittmatter, 2007). The semaphorin/CRMP signaling pathway involves phosphorylation of CRMPs via various kinases including Rho-kinase, CDK5 or GSK3β, which leads to microtubule destabilization and axon retraction (Yamashita & Goshima, 2012; Sasaki *et al*, 2002; Balastik *et al*, 2015). In addition to their role in mediating semaphorin intrinsic cell responses, CRMPs have been reported to bind dynein and kinesin, and modulate their function (Arimura *et al*, 2009; Rahajeng *et al*, 2010). Several studies have demonstrated the involvement of CRMPs in neurodegenerative diseases and neuronal injury (Charrier *et al*, 2003; Nagai *et al*, 2017; Yamashita & Goshima, 2012; Jang *et al*, 2010). Specifically, CRMP4 expression levels were found to be elevated in the $SOD1^{G93A}$ mouse spinal cord, and were suggested to promote MN death (Duplan *et al*, 2010; Valdez *et al*, 2012; Nagai *et al*, 2015). Interestingly, mutations in CRMP4 are associated with ALS (Blasco *et al*, 2013). However, the mechanism of CRMP4 mediated-MN cell death in ALS is unknown.

Here, we identify a novel mechanism by which CRMP4 mediates MN toxicity in ALS. We discover a CRMP4-dependent retrograde signal in ALS motor neurons that facilitates MN loss. This process is mediated by alterations of CRMP4 expression and the formation of a CRMP4-dynein complex via a specific motif in the CRMP4 protein in a subtype of ALS diseased axons.

Results

Alterations in CRMP4 protein levels along ALS diseased motor unit

Increased CRMP4 levels in MN cell bodies of the $SOD1^{G93A}$ ALS mouse model were previously reported to be toxic to MNs and lead to cell death (Duplan *et al.*, 2010). Specific mutations in the N-terminus of CRMP4 are associated with ALS in patients (Duplan *et al*, 2010; Valdez *et al*, 2012; Nagai *et al*, 2015). However, how CRMP4 mediates its toxicity in ALS MNs remains unknown. To address this, we first measured CRMP4 protein levels in the spinal cord of human ALS patients (Figure 1 A-B). Consistent with the published results from the $SOD1^{G93A}$ ALS mice model (Duplan *et al.*, 2010), we observed a significant 2.5-fold increase in the relative

CRMP4 expression in sALS patient compared to non-diseased controls (mean: healthy 1.285 ± 0.184; sALS patient 2.571 ± 0.137) (Figure 1 A, B). This increase was also prevalent in $SOD1^{G93A}$ mice spinal cord, as the total number of cells expressing CRMP4 in the $SOD1^{G93A}$ P90 spinal cord compared to their littermate control was elevated (Figure 1C, D) (mean: WT 4.54% ± 4.4%; $SOD1^{G93A}$ 26.43% ± 3.04%). Next, we determined the expression levels of CRMP4 in the distal part of the motor neuron: I) Intra muscular axons and II) NMJs. Unexpectedly, our analysis in human intra-muscular nerves from sALS patients, revealed a significant 28% decrease in CRMP4 levels within neurofilament heavy chain (NFH) positive axons compared to healthy controls and a similar non-significant trend in MBP positive Schwann cells (Figure 2 A,B) (Appendix Figure S1 A,B) (mean intensity: Non-ALS 1.00 ± 0.097; ALS 0.719 ± 0.108). Furthermore, analysis of P90 gastrocnemius muscles (GC) revealed a decrease in the number of NMJs expressing CRMP4 in $SOD1^{G93A}$ mice compared to the WT control (Figure 2 C,D) (the mean percentage of P90 NMJs expressing CRMP4: WT 90.6595% ± 4.78%; $SOD1^{G93A}$ 60.29% ± 9.00%). Interestingly, we detected early partial NMJ degeneration in CRMP4-negative NMJs, suggesting an active role for CRMP4 in preservation of distal axons (Figure 2 C,E) (the mean percentage of P90 partially-innervated $SOD1^{G93A}$ NMJs: CRMP4 positive 33.33% ± 16.67%; CRMP4 negative 91.67% ± 8.33%). Lastly, we monitored CRMP4 expression levels in WT and $SOD1^{G93A}$ P90 sciatic nerves by immunostaining. We detected a 3-fold increase in CRMP4 signal in sciatic nerve axons (NFH-positive), and a moderate 70% increase in CRMP4 signal also in GFAP positive cells in $SOD1^{G93A}$ mice compared to the controls (Figure 2 F,G; Appendix Figure S1 C,D) (mean area: WT 1.00 ± 0.146; $SOD1^{G93A}$ 2.817± 0.32)(mean area: WT 0.763 ± 0.127; $SOD1^{G93A}$ 1.415± 0.25). Western blot analysis of $SOD1^{G93A}$ and WT P90 sciatic axoplasm confirmed this overall increase in CRMP4 levels in ALS sciatic nerves (Figure 2 H,I) (mean: WT 0.56 ± 0.11; $SOD1^{G93A}$ 1.22 ± 0.14). Thus, our data thus far reveal that, while the expression levels of CRMP4 increase in MN cell bodies and proximal nerves, the opposite trend occurs in the distal/terminal parts of the MN and in NMJ of ALS-diseased MNs. This suggests that in ALS, distal-CRMP4 is mislocalized into proximal axons and cell bodies.

CRMP4 protein mislocalization via Dynein dependent activity

To investigate the potentially disease-relevant function of this intracellular mislocalisation of CRMP4, we utilized human iPSC-derived MNs (iPS-MN) from healthy controls and C9orf72-ALS patients (Tank *et al*, 2018) and plated them in microfluidic chambers (MFCs). First, we immunostained for the neuronal/axonal

markers NFH and Tau, along with the MN-specific marker HB9, to validate the MN cell identity (Appendix Figure S2 A-F). Then, we performed immunostaining for CRMP4 to assess changes in its levels in distal axons (Figure 3 A-D). Our analysis revealed no difference in CRMP4 intensity levels between healthy and C9orf72 iPS-MN axons in this system (Figure 3 A,B). In our previous study, we demonstrated that muscle-secreted Sema3A leads to NMJ disruption and axonal degeneration in ALS (Maimon *et al*, 2018). The canonical pathway for CRMP activation involves Sema3A-NRP-PlexinA interactions. Therefore, we considered whether CRMP4 requires stress activation for differential, disease-relevant mislocalization in MNs cultures and asked whether Sema3A treatment might differentially affect CRMP4 levels in ALS iPS-MNs versus Healthy iPS-MNs. We found that exposing distal axons to Sema3A for 8 hours led to significant increase in CRMP4 intensity specifically in axons of C9orf72 MNs (mean: Healthy 0.7 ± 0.05; Healthy+Sema3A 0.75 ± 0.047; C9orf72 0.61 ± 0.03; C9orf72+Sema3A 1.27 ± 0.16) (Figure 3 A,B). Given that CRMP4 levels were specifically high in somata and proximal axons of ALS patients and $SOD1^{G93A}$ mice, we tested the CRMP4 levels in somata and proximal axons of C9orf72 and healthy iPSC-MNs following distal Sema3A treatment. We used Cholera toxin B-647 (CTX) retrograde tracing to specifically examine CRMP4 levels in proximal axons and soma parts of neurons that send their axons into distal compartment of MFC (Figure 3C). Looking specifically at this neuronal population, we detected an increase in CRMP4 intensity post Sema3A treatment in C9orf72 iPS-MN soma and proximal axons but not in healthy iPS-MN controls (Figure 3 D-G)(CRMP4 mean intensity in somata area, measured by GAPDH outline: Healthy 1.00 ± 0.128; Healthy+Sema3A 1.222 ± 0.148; C9orf72 1.00 ± 0.078; C9orf72+Sema3A 1.258 ± 0.068;) (CRMP4 mean intensity proximal axons: Healthy 1.00 ± 0.066; Healthy+Sema3A 1.048 ± 0.059; C9orf72 1.00 ± 0.093; C9orf72 +Sema3A 1.302 ± 0.11).

CRMPs have been reported to bind to the dynein motor protein and modulate its function (Arimura *et al*, 2009; Rahajeng *et al*, 2010). Since distal exposure to Sema3A led to CRMP4 elevation in the ALS diseased MN soma, we speculated that CRMP4 undergoes retrograde transport mediated by dynein. Therefore, we examined CRMP4 levels in the cell bodies and proximal axons of healthy and C9orf72 iPS-MNs that were distally exposed to Sema3A with or without the presence of the dynein inhibitor, Ciliobrevin D (Herein: Dyn-In)(Firestone *et al*, 2012) (Figure 3 D-G). Inhibiting dynein completely blocked Sema3A-induced increase in CRMP4 levels in C9orf72 iPS-MNs axons and somata (Figure 3 D-G; Appendix Figure S3 A,B) (CRMP4 mean intensity somata - measured by GAPDH outline:

Healthy+Sema3A 1.222 ± 0.148; Healthy+Sema3A+Dyn in 1.161 ± 0.067; C9orf72+Sema3A 1.258 ± 0.068; C9orf72+Sema3A+Dyn in 0.787 ± 0.088) (CRMP4 mean intensity proximal axons: Healthy+Sema3A 1.048 ± 0.059; Healthy+Sema3A+Dyn in 1.087 ± 0.089; C9orf72 +Sema3A 1.302 ± 0.11; C9orf72 +Sema3A+Dyn in 0.655 ± 0.036). We did not observe this effect in the presence of Dyn-In alone (Appendix Figure S3 A,B). Furthermore, to validate that distal Sema3A treatment has effect on MN soma, we quantified the cell body area (by measuring CTX signal outline) and found that C9orf72 Sema3A-treated MNs exhibit smaller soma areas compared to untreated or healthy MNs cultures (Appendix Figure S3 C). Here again, when dynein activity was inhibited prior to Sema3A application, this effect was abolished (mean area: Healthy untreated 302 ± 29; Healthy+Sema3A 285 ± 15; Healthy+Sema3A+Dyn-In 296 ± 18; C9orf72 untreated 314 ± 10; C9orf72+Sema3A 263 ± 10; C9orf72+Sema3A+Dyn-In 318 ± 12) (Appendix Figure S3 C). Importantly, no differences were monitored post application of Dyn-In alone in both healthy and disease conditions. These data indicate that the elevation in CRMP4 in cell bodies and in proximal axons of ALS-diseased neurons is mediated by dynein, likely by binding to axonal CRMP4 and subsequent retrograde transport to the cell body.

A specific CRMP4 motif mediates the CRMP4-dynein-dynactin interaction

CRMP2 members were previously found to bind the dynein motor protein (Arimura *et al*, 2009). Arimura et al. also characterized two specific domains in the CRMP2 protein that are responsible for dynein binding (Arimura *et al*, 2009). Since CRMP2 and CRMP4 share substantial sequence similarity, we hypothesized that the dynein-binding domains (100aa-150aa) of CRMP2 would play a similar role in CRMP4. Following this, and on the basis of the CRMP4 protein 3D structure (PDB code 4CNT) (Ponnusamy *et al*, 2014) (Figure 4A), we overexpressed full length GFP-CRMP4 or CRMP4 lacking amino acids 100-150 (GFP-CRMP4Δ100-150) in COS7 cells, and immunoprecipitated the endogenous dynein intermediate chain (DIC). Western blot analysis of these fractions revealed a clear interaction of DIC with full-length GFP-CRMP4 but not with GFP-CRMP4Δ100-150 (Figure 4B) (mean: GFP-CRMP4 1.473± 0.373; GFP-CRMP4Δ100-150 0.009± 0.001). Since a large deletion in the CRMP4 protein sequence may result in its misfolding and dysfunction, we pursued an alternative strategy by generating small peptides to cover the potential dynein-binding motif, and test if this could block dynein binding to CRMP4. We designed four short peptides within the 50 amino acid domain, which exhibit the potential to block CRMP4-dynein interaction, based on the protein structure.

Importantly, the peptide sequences were designed to avoid an overlap with CRMP4 homo-tetramer interfaces, likely preventing a disturbance to the protein's homomeric assembly (Figure 4A). To test the peptides activity, we pre-incubated a mixture of peptides 1-4 with lysate from GFP-CRMP4 overexpressing COS7 cells. This process significantly reduced the CRMP4-DIC interaction (Figure 4 B,C; mean: GFP-CRMP4 1.473± 0.373; GFP-CRMP4 + peptides 0.3± 0.05). We also examined CRMP4 interaction with dynactin (p150), a dynein activator, in COS7 cells overexpressing Flag-tagged CRMP4. After an overnight incubation of cell lysate with peptides 1-4, we pulled-down Flag-CRMP4 and blotted for dynactin (p150). Application of the peptide mixture resulted in a dramatic decrease in CRMP4 binding to dynactin (Figure 4 D,E)(mean: control 0.77± 0.1; All Pep 0.17± 0.06). We also determined whether introducing the individual peptides might be sufficient to also block the CRMP4-dynactin interaction. Using the same assay, we incubated each peptide separately, and found that only peptide-4 had a mild but significant ability to block CRMP4 interaction with dynactin (Figure 4F,G) (mean: control 1.92 ± 0.2; peptide-1 1.44 ± 0.3; peptide-2 1.34 ± 0.3; peptide-3 1.8 ± 0.8; peptide-4 1.13 ± 0.14). Hence, although peptide-4 was sufficient to block CRMP4-dynactin binding, blocking CRMP4-dynactin complex formation requires a combination of all four peptides. Lastly, we generated a genetic tool to block the CRMP4-dynein interaction using a plasmid with the CRMP4-dynein binding motif sequence (corresponding to a.a 100-150 of CRMP4) and determined whether it could act in a dominant-negative manner. We transfected COS7 cells with GFP or GFP-expressing the 50aa sequence (GFP-50aa), then extracted the cells and assayed for CRMP4 that co-purified with the dynein intermediate chain (DIC) via immunoprecipitation. Our Western blot analysis revealed weaker interaction of CRMP4 with dynein in the presence of GFP-50aa overexpressing cells compare to the control (mean: GFP CRMP4 1.00 ± 0.10; GFP-50aa 0.54 ± 0.11) (Figure 4 H,I). Thus, amino acids 100-150 in the CRMP4 protein are sufficient and essential for CRMP4/dynein/dynactin binding.

Enhanced CRMP4-dynein complex formation in ALS Diseased MNs

Our data thus far suggest that CRMP4 levels are: 1) increased in the cell soma and 2) decreased in the NMJs and distal axons of ALS diseased MNs (Figure 1, Figure 2). We further demonstrated that CRMP4 mislocalization in ALS-diseased MNs can be facilitated by Sema3A and is mediated by dynein (Figures 3 and Figure 4). Since our previous report suggests elevations in Sema3A secretion from ALS muscles (Maimon *et al*, 2018), we predicted an increase in CRMP4-dynein complex formation along the axons of ALS models. To test this, we first extracted sciatic nerves

axoplasm from WT and SOD1^{G93A} P90 mice, and measured the levels of CRMP4 that co-purified with the dynein intermediate chain (DIC) *in vivo* using immunoprecipitation. We found a stronger interaction of DIC with CRMP4 in the SOD1^{G93A} mice compared with the control (Figure 5 A, B) (mean: WT 0.28 ± 0.11; SOD1^{G93A} 1.48 ± 0.62). Notably, transfecting cells with CRMP4 that carries an ALS-associated mutation, I141V, also enhanced the formation of the CRMP4-dynein complex (Figure 5 C,D) (mean: WT CRMP4 1.00 ± 0.207; Mutated CRMP4 1.625 ± 0.116). Importantly, I141V is located in the same dynein binding motif in the CRMP4 protein, suggesting a CRMP4 gain of toxic function in ALS.

To further characterize CRMP4-dynein interactions in ALS, we attempted to track CRMP4-GFP retrograde movement in healthy and ALS diseased MN axons. However, overexpressing CRMP4-GFP resulted in a uniformly diffuse distribution (Appendix Figure S4). Thus, in order to demonstrate retrograde transport of endogenous CRMP4 we immunostained distinct cellular compartments (dynein and CRMP4) using Proximity Ligation Assay (PLA), as previously performed (Olenick *et al*, 2019). First, by using PLA, we observed that indeed there is an increase in the CRMP4-dynein colocalization along cultured WT MNs axons, post Sema3A treatment compared to untreated WT cultures (Figure 5E). Importantly, this colocalization was twice as high in the Sema3A-treated SOD1^{G93A} MNs axons (Figure 5 E,F). Furthermore, when comparing co-localization patterns of the CRMP4-dynein puncta in human iPS-MNs in the presence or absence of Sema3A, we obtained similar results: In naive, untreated axons, the number of CRMP4-dynein puncta was similar between healthy and C9orf72 iPS-MNs. However, following Sema3A treatment, the number of CRMP4-dynein puncta in *C9orf72* axons was significantly higher compared to treated healthy control (Figure 5 G,H) (mean puncta per axon: Healthy untreated 0.032 ± 0.004; Healthy+Sema3A 0.062 ± 0.006; C9orf72 untreated 0.082 ± 0.004; C9orf72+Sema3A 0.344 ± 0.026). Next, in order to determine whether the formation of CRMP4-dynein complexes in MN axons is reversible, we aimed to block the CRMP4-dynein interaction in iPS-MN distal axons. To this end, we plated healthy and C9orf72 iPS-MNs in MFCs and exclusively introduced a mix of all peptides (1-4) into axons in the distal compartment. Using TAMRA peptides as a positive control for uptake, we observed that peptides 1-4 peptides were successfully taken up by distal axons (Appendix Figure S5 A,B). Strikingly, application of peptides 1-4 significantly interfered with the interaction of CRMP4 and dynein in distal *C9orf72* iPS-MN axons as determined by PLA. CRMP4-dynein interaction in healthy iPS-MN remained unaffected by either Sema3A,

peptides 1-4, or by both (Figure 5 G,H)(mean puncta per axon: Healthy+Sema3A 0.062 ± 0.006; Healthy+Sema3A+peptide 0.063 ± 0.006; C9orf72+ Sema3A 0.344 ± 0.026; C9orf72+ Sema3A+ peptide 0.067 ± 0.009). No differences were monitored when peptides were inserted without Sema3A activation in both conditions (Figure 5 G,H)(mean puncta per axon: Healthy untreated 0.032 ± 0.004; Healthy+peptides 0.056 ± 0.004; C9orf72 untreated 0.082 ± 0.004; C9orf72+peptides 0.080 ± 0.005). Together, we have demonstrated both *in vivo* and *in vitro* that the CRMP4-dynein interaction is elevated in ALS-mutated MN axons. Importantly, this strong interaction can be blocked in ALS MN axons by interfering with the CRMP4-dynein binding domain using both genetic and pharmacological tools.

The CRMP4-dynein complex facilitates selective neuronal loss in ALS

MNs undergo apoptosis and degenerate in ALS (Reyes et al, 2010). Downregulation of CRMP4 was previously suggested to inhibit neurodegeneration *in vitro* and *in vivo* in ALS models (Charrier *et al*, 2003; Duplan *et al*, 2010). Thus, we examined whether enhancement of the CRMP4-dynein interaction by Sema3A would lead to neuronal cell death in ALS. Similar to the experimental design in Figure 3C, we applied CTX to the distal compartment of the MFCs in order to label only the cell bodies of neurons whose axons traversed into the distal compartment. The number of CTX^+ iPS-MNs were quantified before and 2 days after Sema3A was applied to the distal compartment. Our analysis did not detect any significant loss of CTX^+ cells in healthy iPS-MNs in response to Sema3A, whereas in *C9orf72* iPS-MNs we detected a ~25 percent decrease in CTX^+ MNs upon treatment with Sema3A (Figure 6A-C). Similarly, applying Sema3A to spinal cord cultures from $SOD1^{G93A}$ embryos resulted in a ~30% reduction in CTX^+ MNs 3 days after treatment, compared with ~5% in the control and WT explants (Figure 6D-E; Appendix Figure S6) (mean fold change over control: Sema3A 0.68 ± 0.06; control 1 ± 0.04). In order to determine whether distal stress such as Sema3A application triggers MN loss in ALS-diseased MNs via retrograde signaling, we used dynein inhibitor to block all retrograde transport events (Firestone *et al*, 2012). Inhibiting retrograde transport in the distal axon prevented MN loss in the $SOD1^{G93A}$ primary cultures (Figure 6D,E; Appendix Figure S6 A-E) (mean fold change over control: Sema3A + Dyn-In 0.92 ± 0.09; control 1 ± 0.04). Sema3A was previously shown to internalize together with its receptor, Plexin A1 (PLXNA1) in a dynamin-dependent manner (Castellani *et al*, 2004; Fournier *et al*, 2000). To further determine whether endocytosis of Sema3A is important for the apparent retrograde death signal, as shown before in different neurons (Wehner et al., 2016), we applied Dynasore, a dynamin-dependent endocytosis inhibitor (Macia

et al, 2006), to the distal axons prior to application of Sema3A. Inhibiting Sema3A+PLAXNA1 (Appendix Figure S7) internalization did not inhibit the loss of $SOD1^{G93A}$ CTX^+ MNs (Figure 6E; Appendix Figure S6) (mean fold change over control: Sema3A + Dynasore 0.71 ± 0.01; control 1 ± 0.04). Thus, Sema3A internalization at the distal axons, is not required for the observed toxicity. Importantly, interfering with the CRMP4-dynein interaction by introducing peptides 1-4 into diseased iPS-MN axons prior to applying Sema3A completely abolished the CTX^+ signal loss (mean: Control 0.97± 0.009; Sema3A 0.813± 0.036; Sema3A + Pep 0.94± 0.019) (Figure 6 F,G). Our findings demonstrate that death of ALS MNs following Sema3A application can be prevented by inhibiting the formation of CRMP4-dynein complexes.

We further examined whether impairing the CRMP4-dynein interaction *in vivo* reduces MN death, which is a hallmark in the $SOD1^{G93A}$ mouse model. To this end, we chose to prevent CRMP4-dynein interaction using intrathecal injections of AAV9 viruses to insert CRMP4 dominant negative construct (Figure 4 H,I) into spinal cord MNs. First, to demonstrate injection efficacy, we immunostained spinal cord and sciatic nerve tissues that were infected with a control AAV9-GFP, by intrathecal injections (Appendix Figure S8 A) and monitored the percentage of infected neurons by analyzing colocalization of the neuronal markers NeuN or NFH with GFP in spinal cords and axons along the sciatic nerves (Appendix Figure S8 B,D). We found that 65% of spinal cord neurons as well as 50% sciatic nerve axons expressed GFP signal in AAV9-GFP injected mice compared to non-injected control (Appendix Figure S8 C,D) (Infected SC mean: Non injected 0.25% ± 0.19%; AAV9-GFP 70.31% ± 0.97% ; Infected SN mean: Non injected 0.25% ± 0.163%; AAV9-GFP 53.98% ± 4.233%). We then delivered AAV9-GFP-50aa/AAV-GFP as a dominant negative approach, into pre-symptomatic ~P60 $SOD1^{G93A}$ CSF by lumbar intrathecal injection and monitored for the activation of the apoptotic marker caspase 3 (Pasinelli *et al*, 1998; Porter, 1999; Reyes *et al*, 2010) 4 weeks post injection (Figure 7A-E). Importantly, GFP signal was detected in similar number of spinal cord neurons and in similar intensity in both AAV treatments, meaning no difference in infection effectiveness between the GFP and GFP-50aa constructs (Appendix Figure S8 E,F)(Infected cells mean: AAV9-GFP 70.31% ± 4.024%; 50aa-AAV9-GFP 76.38% ± 2.965%) (GFP

intensity mean: AAV9-GFP 3955 ± 318; 50aa-AAV9-GFP 3625 ± 383). We measured the degree of activated caspase 3 in P90 SOD1^{G93A} and compared it to the age matched control. As expected, ~90% of NeuN positive cells with MN morphology in the ventral horn were positive for activated caspase 3 in the spinal cord of SOD1^{G93A} mice, while only few caspase 3 positive neurons were detected in the control mice (Figure 7A,B) (mean: WT 12.18 ± 5.666; SOD1^{G93A} 92.67 ± 3.167). Injection with AAV9-GFP-50aa resulted in a ~25% decrease in the percentage of activated caspase 3 positive cells in the spinal cord of SOD1^{G93A} mice, compared to injection with AAV9-GFP (Figure 7 C,D)(mean: AAV9-GFP 84.44% ± 1.47%; AAV9-GFP-50aa 73.24% ± 0.39%). Additionally, the number of NeuN positive cells in the ventral horn of the spinal cord was significantly higher in the 50 aa injected group compared with GFP control (Figure 7 E) (mean: AAV9-GFP 1 ± 0.12 AAV9-GFP-50aa 1.37 ± 0.12).

Taken together, our *in vivo* and *in vitro* data demonstrate that a CRMP4-dynein complex contribute to motor neuron loss in ALS disease. Importantly, this process is reversible and can be prevented by blocking the CRMP4 and dynein interaction.

Discussion

Duplan et al., previously reported that CRMP4 is elevate in SOD^{G93A} MNs both *in vivo* and *in vitro* and lead to their loss. By reducing CRMP4 levels the group demonstrated protective effect on MN health (Duplan *et al*, 2010). However, the mechanism by which CRMP4 mediates MN toxicity, its involvement in other ALS models and its relevance to human ALS disease were unknown. In this work we discover subcellular alterations in CRMP4 levels in sALS human patients, C9orf72 human derived MNs and in the SOD^{G93A} mice CRMP4 alterations dependent on dynein activity. Specifically, CRMP4-dynein interactions are mediated by amino acids 100-150 in the CRMP4 protein, a region in which mutation was indeed correlated with ALS (Blasco *et al*, 2013). Notably, CRMP4-dynein complexes are enriched in ALS diseased MNs, and lead to ~25% cell death observed in ALS diseased spinal cord. Finally, we show that blocking the CRMP4-dynein interaction rescued this MN population, both *in vitro* and *in vivo* (Figure 7F). These results pose many important open questions:

<u>What is the cause for CRMP4 alterations in ALS-diseased MN axons?</u>

Here, we reported that CRMP4 is elevated in the soma of several ALS model MNs but is decreased near distal axons. We further demonstrated that Sema3A facilitates an increase in CRMP4 protein levels specifically in ALS diseased MN somata and proximal axons. Since in our previous report we demonstrated that ALS disease muscles secrete Sema3A, we assume that CRMP4 elevations in somata and proximal axons are due to the nearby presence of Sema3A. However, the mechanism responsible for the permanent elevation of CRMP4 specifically in ALS-diseased MNs is unknown. miRNA downregulation and defects in local protein synthesis are common features in several ALS models (Haramati *et al*, 2010; Costa & Willis, 2018). Along with that, Sema3A was shown to induce axonal local synthesis in several neuronal systems (Manns *et al*, 2012; Wu *et al*, 2005; Campbell & Holt, 2001; Cagnetta *et al*, 2019, 2018). Thus, we hypothesize that the permanent elevation in CRMP4 that we observed in diseased MN somata and proximal axons are possibly due to increase in axonal protein synthesis. Specifically, our recent published work suggests that miR126-5p is downregulated in both muscles and MN axons in several ALS models (Rotem *et al*, 2017; Maimon *et al*, 2018). Thus, it is tempting to speculate further that miR126-5p downregulation mediates CRMP4 increases in ALS-diseased MNs via local protein synthesis and consolidation of retrograde death signals in ALS models. Another possibility for CRMP4 alterations in ALS disease is a proteolytic degradation of CRMP4 at the injured site of the neuron, as has been shown before (Jang *et al*, 2010). Further experiments are needed to test the probability of those ideas.

How does CRMP4-dynein activate caspase 3 in ALS diseased MNs?

Our data further suggest that CRMP4 forms complexes with dynein along ALS-diseased MNs and leads to their loss via a caspase 3-dependent cascade. However, it is still not clear whether CRMP4 itself activates the apoptotic program or whether it plays a regulatory role in recruiting the death complex. Since CRMP members have not yet been reported to act as transcription factors, we assume that CRMP4 is indeed a critical part of a retrograde signaling complex that might contain additional proteins. For example, DLK regulation of JNK and c-Jun might also be a part of this death signal mediated by Sema3A in ALS MNs, since it was previously shown that both DLK and JNK signaling are elevated in ALS models and that they are part of a retrograde death signal (Ghosh *et al*, 2011; Siu *et al*, 2018; Escudero *et al*, 2019; Perlson *et al*, 2010). Another possibility is that the neurotrophic receptor $p75^{NTR}$ is also involved in this process. $p75^{NTR}$ regulates a diverse range of cellular functions including axon pruning (Singh *et al*, 2008) and neuronal death (Bamji *et al*, 1998;

Kenchappa *et al*, 2010; Pathak *et al*, 2018). $p75^{NTR}$ is retrogradely transported along the axon (Deinhardt *et al*, 2006; Cosker & Segal, 2014; Harrington & Ginty, 2013) and plays a role in generating a retrograde apoptotic signal that activates JNK (Kenchappa *et al*, 2010). It is noteworthy that the activity of Sema3A and its receptor was previously linked to $p75^{NTR}$ (Ben-Zvi *et al*, 2007). Another possible candidate that was shown to be coupled with Sema3A is PTEN (Chadborn *et al*, 2006). Furthermore, it was established that the $p75^{NTR}$-dependent apoptosis signal is promoted by PTEN activation (Song *et al*, 2010). Thus, future experiments should examine whether PTEN, $p75^{NTR}$, and JNK indeed participate in Sema3A-dependent retrograde death signals in ALS.

CRMP4 gain of toxicity in ALS disease

CRMP4 overexpression has been suggested to cause MN death in ALS models (Charrier *et al*, 2003; Duplan *et al*, 2010). Furthermore, a *CRMP4* mutation was associated with ALS in patients (Blasco *et al*, 2013), However, the mechanism of CRMP4 toxicity in ALS MNs is unknown. Here, we demonstrate a specific mechanism by which CRMP4 toxicity to MNs is dependent on dynein activity. Moreover, we demonstrate that amino acids 100-150 of CRMP4 are responsible for the CRMP4 and dynein interaction. Importantly, the ALS associated mutation in CRMP4 is located in this motif. Our data show a stronger dynein interaction for the mutant CRMP4, which is in accordance with CRMP4 gain of toxicity. Alternatively, CRMP4 has been documented before, in a number of experimental models to elevate post neuronal injury (near injury site). Thus, it is possible that the results in this manuscript reflect a response of motor neurons to stress rather than an ALS-specific mechanism (Jang *et al*, 2010). Additional studies will be needed to dissect in detail the mutant CRMP4 activity in ALS-diseased MNs.

Materials and Methods

Animals

$SOD1^{G93A}$ (Stock No. 002726) mice were originally obtained from Jackson Laboratories, and maintained by breeding with C57BL/6J mice. B6;129S6-$ChAT^{tm2(cre)Lowl}$/J (Stock No. 006410) and B6;129S6Gt(ROSA)26 $Sor^{tm14(CAG-tdTomato)Hze}$/J (Stock No. 007908) mice were originally obtained from Jackson Laboratories. Animals were cross-bred in the Tel-Aviv SPF animal unit to yield homozygous ChAT::$Rosa^{tdTomato}$ mice. The ChAT::$Rosa^{tdTomato}$ colony was

maintained by in-breeding males and females from the colony. The ChAT::Rosa^{tdTomato} colony was cross-bred with SOD1^{G93A} to yield SOD1$^{G93A/ChAT::tdTomato}$ mice. C57BL/6 J mice were used as a WT mouse strain. Mice were genotyped using the PCR reaction (KAPA Bio Systems - Wilmington, MA, USA). DNA samples were generated from mouse ear or tail. Animal experiments were performed under the supervision and approval of the Tel-Aviv University Committee for Animal Ethics.

iPSc Cultures

Healthy/Control iPSC lines, provided by Dr. Sami Barmada, were created and characterized as before (Tank *et al*, 2018). Two lines from fALS patients carrying the C9orf72 mutation, and two lines from healthy controls, were used for all experiments.

Name	**Age donated**	**Age of onset**	**Gender**	
ALS883	51	49 (Lumbar)	**M**	(>44 repeats per Athena 7/26/2012
ALS312	54	52 (Lumbar)	**M**	(44 and 2 repeats) by Athena Diagnostics 10/03/2012
Control746	58		**M**	Healthy
Control1021	54		**F**	Healthy

Colonies were groomed daily until each well of the 6-well plate was between 30% and 40% confluence and no spontaneously differentiated cells were observed. At this point, we used the direct iMN" (diMN) differentiation in monolayers from hiPSCs protocol published by Cedar Sinai and approved by Dhruv Sareen (Protocol number: CSMNC-SOP-C-005) for our experiments. Briefly, we induced MN differentiation by MN Differentiation Stage 1 media: prepared with – IMDM (LifeTech), F12 (LifeTech), NEAA (Gibco), B27 (LifeTech), N2 (LifeTech), PSA (LifeTech), LDN193189 0.2 μM (Selleck), SB431542 10 μM (Tocris), and CHIR99021 3 μM (Cayman Chemicals). The media was gently added to the wells, and colonies were grown with it for 5 days. MN differentiation Stage 2: At day 6 the colonies were dissociated, using accutase, and 100K cells were plated in the proximal compartment of our micro fluidic device. Stage 2 media, which contains IMDM, F12, NEAA, B27, N2, PSA, LDN193189 0.2 μM (Selleck), SB431542 10 μM (Tocris), and CHIR99021 3 μM (Cayman Chemicals), All-trans RA 0.1 μM (Stemgent), and SAG 1 μM (Sonic Hedgehog Agonist – Cayman Chemicals) media was added to both the distal and proximal compartments of the

MFC and refreshed every 2 days until day 11. MN differentiation Stage 3: At day 12 the media was changed to stage 3 media prepared with IMDM, F12, NEAA, B27, N2, PSA, Compound E 0.1 μM (Calbiochem), DAPT 2.5 μM (Cayman Chemicals), db-cAMP 0.1 μM (Millipore), Alltrans RA 0.5 μM (Stemgent), SAG 0.1 μM, Ascorbic Acid 200 ng/ml (Sigma), BDNF 10 ng/ml (Alomone lab), and GDNF 10 ng/ml (Alomone lab) and was refreshed every 2 days until cells exhibited MN neuronal morphology and positive markers. Human iPSC experiments were performed under the supervision and approval of the Tel-Aviv University Committee for Human Ethics.

Microfluidic chamber preparation

Polydimethylsilxane (PDMS) microfluidic chambers (MFCs) were designed and cast as described previously (Ionescu *et al*, 2016). Briefly, MFCs were fabricated from our designed templates and made from PDMS mixture at 70°C. After the wells were punched, a small 'cave' was made in the explant well near the grooves using a 25G needle, keeping the explant in place. Microfluidic devices were cleaned of surface particles using adhesive tape and were sterilized in 70% ethanol for 15 minutes. Devices were completely dried under sterile conditions using UV radiation, attached to a sterile 60-mm plastic dishes (Nunc) with gentle pressure and margins were sealed with PDMS before incubation at 60°C for 30 minutes to prevent the chamber from detaching. The wells and channesl were filled with 150μL of 1.5 ng/mL polyornithine (P-8638, Sigma) in PBS overnight, and then replaced with 150 μL laminin (L-2020, Sigma), 1:333 in deionized distilled water (DDW) overnight. One day before plating the spinal cord explant, laminin was replaced with explant medium containing Neurobasal (Life Technologies) supplemented with 2% B27 (Invitrogen), 1% penicillin-streptomycin (Biological Industries), 1% Glutamax (Life Technologies), 25 ng/mL brain-derived neurotrophic factor (Alomone Labs), until the day on which co-culturing began.

Motor neuron cell culture

Primary spinal cord neurons were cultured using E12.5 mouse embryos of either sex as previously described (Zahavi *et al*, 2015). Briefly, spinal cords were excised, trypsinized, and triturated. Supernatant was collected and centrifuged through a 4% BSA cushion. The pellet was resuspended and centrifuged through an Optiprep gradient (10.4% Optiprep (Sigma-Aldrich), 10 mM Tricine, 4% glucose) for 20 min at 760 x g with the brake turned off. Cells were collected from the interface, washed once in complete medium, and then plated in coated growth chambers. Cells were

maintained in Complete Neurobasal Medium (Gibco) containing B27 (Gibco), 10% (v/v) horse serum (Biological Industries), 25 nM beta-mercaptoethanol, 1% Penicillin-Streptomycin (PS; Biological Industries), and 1% GlutaMAX (Gibco) supplemented with 1 ng/mL Glial-Derived Neurotrophic Factor (GDNF), 0.5 ng/mL Ciliary Neurotrophic Factor (CNTF), and 1 ng/mL Brain-Derived Neurotrophic Factor (BDNF), (Alomone Labs). Prior to plating, growth plates were coated with 1.5 g/mL poly D-L-ornithine (PLO; Sigma-Aldrich) overnight at 37 °C and with 3 µg/mL Laminin (Sigma-Aldrich) for 2 hours at 37 °C. For immunofluorescence staining, 10,000 cells were plated on cover slides in 24-well plates. Cells were grown at 37 °C in 5% CO_2.

Spinal cord explants

Spinal cords were dissected from E12.5 mouse embryos of both sexes, either using HB9::GFP or $SOD1^{G93A}$ stripped of meninges and dorsal root ganglia. The ventral horn was separated from the dorsal horn by longitudinal cuts along the spinal cord, and transverse sections up to 1 mm were placed in the explant well**.** Prior to plating, growth chambers were coated with 1.5 g/mL PLO overnight at 37 °C and 3 µg/mL Laminin overnight at 37 °C. Explants were maintained in Spinal Cord Explant Medium containing Neurobasal, 2% B27, 1% PS, and 1% GlutaMAX, supplemented with 25 ng/mL BDNF. Explants were grown at 37 °C in 5% CO_2.

Fluorescence microscopy and image analysis

All confocal images were captured using a Nikon Ti microscope equipped with a Yokogawa CSU X-1 spinning disc and an Andor iXon897 EMCCD camera controlled by Andor IQ3 software. All live-imaging assays were performed in a humidified incubation chamber at 37°C, 5% CO_2. Images were analyzed using ImageJ software.

Rertrograde labeling of cell bodies in the MFC

Alexa Fluor 647-conjugated Cholera toxin subunit B (CTX; Thermo-Fisher C-347777) at 500 ng/mL was applied to the distal compartment of an MFC system while maintaining a higher liquid volume in the proximal compartment to prevent unspecific labeling by diffusion. After 8 hours, only somata whose axons traversed to the distal compartment were labeled.

Recombinant Sema3A application

Recombinant Sema3A (R&D,1250-S3-025) at 500 ng/mL was used in our experiments. We dilute the Sema3A in poor neurobasal (PNB) containing Neurobasal medium (Gibco) with 1% PS and 1% Glutamax.

Retrograde transport inhibition

In order to inhibit dynein-dependent retrograde transport, Cilliobrevin-D (Merck-Millipore, 250401) at 10 μM was applied to the distal compartment of the MFC while maintaining a proximal-to-distal volume gradient.

Inhibition of dynamin-dependent endocytosis

Dynasore (Sigma Aldrich, D7693) at 100nM was added to the distal compartment of the MFC while maintaining a proximal-to-distal volume gradient.

Pull down assays

For the cell cultures pull downs experiments, 2 x 10^6 COS7 cells were plated in 10 cm culture dishes. The following day, cells were transfected using calcium phosphate protocol with Flag-CRMP4/ GFP-CRMP4/ GFP-Delta-CRMP4/ Mutated-Flag-CRMP4/ AAV9-GFP/ AAV9-GFP-50aa vector. The next day, cells were lysed, and proteins were extracted using lysis buffer containing PBS, 1% Triton- 100X, and 1% protease and phosphatase inhibitors (Roche), followed by centrifugation and collection of the supernatant. At this point, immunoprecipitation preparation of the lysate was precleared with protein-A-agarose beads (Roche). Following overnight incubation with primary anti-flag antibody/anti DIC antibody, complexes were incubated with protein A agarose beads for 2 h at 4 °C and then precipitated and washed with PBS with 0.1% Triton X-100 (Sigma). Proteins were eluted by boiling in sample buffer and then subjected to western blot precipitation analysis with CRMP4/dynactin p150/Flag antibody(Sigma-Alderich F3165)/DIC. We used mouse IgG antibody as a control (SC-2025). For sciatic nerve pull downs, 12 sciatic nerves were pooled for each experiment. Here as well, the P90 sciatic nerve samples were first excised and homogenized in lysis buffer containing PBS and 1% protease and phosphatase inhibitors (Roche), followed by centrifugation and collection of the supernatant. Then we performed the pull-down assay using the technique described above. Under these conditions, pull downs were performed using DIC (Millipore MAB1618) and CRMP4 (Millipore AB5454) antibodies.

Western blotting

Sciatic nerve axoplasm was isolated by excising and cutting sciatic nerves into short segments, followed by detergent-free buffer homogenized with PBS X1 protease and phosphatase inhibitors (Roche), followed by centrifugation and collection of the supernatant. Complete sciatic nerve extracts were achieved in the same manner with

612 the exception of adding 1% Triton X-100. The protein concentration was determined
613 using the Bio-Rad Protein Assay. Protein samples were denatured by boiling in SDS
614 sample buffer and then electrophoresed in 8% polyacrylamide gels (SDS-PAGE).
615 Proteins were transferred to a nitrocellulose membrane and then immunoblotted with
616 appropriate primary antibodies: anti-CRMP4 - 1:2000 (Millipore AB5454) anti-DIC –
617 1:1000 (Millipore MAB1618) anti-p150 1:250 (BD Bioscience 611003) anti-Flag
618 1:4000 (Sigma-Alderich F3165) anti-Tubulin 1:10,000 (ab7291); and anti-tERK
619 1:10,000 (M5670), diluted in 5% (w/v) Skim-milk (BD Difco) in TBS-T, followed by
620 species-specific HRP-conjugated secondary antibodies (Jackson Laboratories) and
621 visualized using a myECL imager (Thermo), according to the manufacturer's
622 instructions. ImageJ software was used for quantification.
623
624 **AAV production**
625 We used AAV serotype 9 (AAV9) for overexpression experiments. The AAV9
626 produced in AAVpro 293T cells (Takara-Clontech, #632273), with the AAVpro®
627 Purification Kit (All Serotypes) from TaKaRa (#6666). For each construct four 15 cm
628 plates were transfected with 20 µg of DNA (AAVplasmid containing the construct of
629 interest and two AAV9 helpers plasmids) using jetPEITM (Polyplus-transfection) in
630 DMEM medium without serum or antibiotics. pAdDeltaF6 and pPHP.S helper vectors
631 were kind gift from Prof. Fainzilber. Medium (DMEM, 20 % FBS, 1 mM sodium
632 pyruvate, 100 U/mL penicillin 100 mg/mL streptomycin) was added on the following
633 day to a final concentration of 10% FBS and extraction was done at three days post
634 transfection. Purification was performed according to the manufacturer's instructions.
635 For all constructs, we obtained titers in the range of 10^{13}- 10^{14} viral genomes/ml.
636
637 **Vector injections**
638 The injection procedure was performed on pre-symptomatic ~P60 mice. Mice were
639 first anesthetized using a mixture of Xylasin and ketamine. Then, a thin incision was
640 performed in the mouse skin in order to expose the area of the L-5 and L-6
641 vertebrae. Next, 5 µL of AAV9-GFP ($6.5X10^{14}$ vg /ml) or AAV-GFP-50aa ($1.21X10^{13}$
642 vg /ml), were injected by intrathecal injection to L5-L6 vertebrae in the spinal cord
643 using a 25 µL Hamilton syringe and a 30G Hamilton needle. All animal
644 experimentations were approved by the Tel-Aviv University Animal Ethics
645 Committee. This method was conducted with the help of Dr. Michael Tolmasov. All
646 the tissues were taken 4 weeks post injection.
647
648 **Human muscle biopsy for intra-muscular nerve staining**

Intra-muscular nerve staining was performed on muscle biopsies from ALS patients and non-ALS patients. All clinical and muscle biopsy materials used in this study were obtained with written informed consent during 2016-2020 for diagnostic purposes followed by research application, approved by the institutional review board. Deltoid, quadriceps or gastrocnemius skeletal muscle samples were excised via open biopsies and pathological analysis was performed at the neuromuscular pathology laboratory at Sheba Medical Center, Ramat-Gan, Israel. All ALS patients were diagnosed with clinically definite or probable ALS according to Awaji criteria (de Carvalho *et al*, 2008) Control muscles included a variation of findings, which were consistent with a diagnosis of normal muscle, severe, chronic ongoing denervation and reinnervation due to spinal stenosis, necrotic autoimmune myopathy, type 2 fiber atrophy due to disuse and overlap myositis syndrome.

Frozen muscle biopsies were cryo-sectioned to 10µm thick slices, mounted onto slides and air dried for 30 minutes in room temperature (RT). Sections were washed in PBS, fixed in 4% PFA for 20 min, and permeabilized with 0.1% Triton, and blocked with 5% goat serum (Jackson Laboratories) and 1 mg/mL BSA (Amresco). Sections were than incubated with appropriate antibodies overnight at 4°C in blocking solution Rabbit anti CRMP4 (Millipore AB5454, 1:250), Chicken anti NFH (Abcam, 1:1,000). Sections were washed again and incubated for 2 hours with secondary antibodies (1:1,000, Jackson Laboratories and ThermoFisher), washed and mounted with ProLong Gold (Life Technologies).

IHC of CRMP4 in human spinal cord tissue

The Dako Autostainer Link 48 (Agilent, USA) was used for all human spinal cord immunohistochemistry. The CRMP4 antibody (Millipore AB5454) was used at 1:700 for 30 minutes at room temperature. Heat induced epitope retrieval was used prior to staining with Dako's EnV Flex Low pH TRS. The Dako Envision Flex Plus Mouse Link Kit (Agilent, USA) to detect the antibody along with the Dako DAB (Agilent, USA). CRMP4 relative expression was semi-quantified by scoring IHC spinal cord sections between 1-3, blindly. 1= Low expression, 2= Middle expression 3= High expression

Sciatic nerve sectioning and immunostaining

Sciatic nerves of P90 mice were isolated and immediately fixed by using 4% PFA followed by 20% sucrose incubation. Then the samples were embedded by freezing in Tissue-Tek® OCT. Next, 10 µm lumbar sciatic nerve sections were prepared using Cryotome™ FSE cryostat (Thermo-Fisher Scientific). Sections were rinsed in PBS,

and then permeabilized with 0.1% Triton X-100, 5% Goat Serum (GS), 1 mg/mL Bovine Serum Albumin IgG, and protease free (BSA) in PBS. Primary antibodies against NFH 1:500(Abcam ab72996/ Covance smi31p/ Covance smi32p) / CRMP4 1:400 (Millipore AB5454) /GFP 1:400 (Abcam ab13970) were diluted in blocking solution, 5% GS, 1 mg/mL BSA in PBS, and incubated overnight at 4°C. Samples were incubated with species-specific fluorescent secondary antibodies for 2 hours at room temperature. ProLong antifade medium (Molecular Probes) was added and the samples were covered with a #1.5, 18×18 mm cover slide.

Spinal cord sectioning and immunostaining

Spinal cord of P90 mice were isolated and immediately fixed by using 4% PFA followed by 20% sucrose incubation. Then the samples were embedded by freezing in TissueTek® OCT. Next, 10 µm lumbar spinal cord sections were prepared using Cryotome™ FSE cryostat (Thermo-Fisher Scientific). Sections were rinsed in PBS, and then permeabilized with 0.1% Triton X-100, 5% Goat Serum (GS), 1 mg/mL Bovine Serum Albumin IgG, and protease free (BSA) in PBS. Primary antibodies against NeuN 1:500 (Milipore MAB377)/ CRMP4 1:400 (Millipore AB5454)/ GFP 1:400(Abcam ab13970)/ activated Caspase 3 1:15 (Biovision 3015-100) were diluted in blocking solution, 5% GS, 1 mg/mL BSA in PBS, and incubated overnight at 4°C. Samples were incubated with species-specific fluorescent secondary antibodies for 2 hours at room temperature. ProLong antifade medium with Dapi (Molecular Probes) was added and the samples were covered with a #1.5, 18×18 mm cover slide.

Immunostaining of cell cultures

Cultures were fixed in 4% paraformaldehyde and permeabilized with 0.1% Triton X-100, 5% GS, 1 mg/mL BSA in PBS. Samples were blocked for 1 hour with blocking medium containing 5% GS and 1 mg/mL BSA in PBS. Primary antibodies against Tau 1:100 (abcam, ab80579) NFH - 1:500 (Sigma-Aldrich N4142), PlexinA1 - 1:100 (Alomone lab, APR-081-F), CRMP4- 1:100 (Millipore, AB5454), GAPDH 1:500 (abcam, ab9484), Tubulin 1:500 (abcam, ab7291), HB9 1:100 (IMGENEX, IMG-6549A) were diluted in blocking solution and incubated overnight at 4°C. Samples were incubated with species-specific fluorescent secondary antibodies for 2 hours at room temperature. For visualizing nuclei in myotubes, DAPI was used. In the MFC, after the staining protocol was completed, the MFC was peeled from the dish by gently pulling it from the proximal to the distal side.

Whole mount NMJ Immunofluorescence staining

Gastrocnemius muscles of P60/ P90 $SOD1^{G93A/ChAT::tdTomato}$ or $WT^{ChAT::tdTomato}$ mice were dissected from mice, washed with cold PBS and cut in longitudinal sections along the fiber before fixed in 4% paraformaldehyde (PFA) in PBS for 15 min at room temperature, while rocking. From fixation until the end of staining protocol (mounting), muscle fibers were washed three times with PBS after each step, except between blocking and primary antibodies staining. After been fixated, muscle fibers were further dissected into smaller section, along fiber orientation. For postsynaptic AChR labelling, the fibers were then stained with αBTX (TMR-α-bungarotoxin; T0195 Sigma) 2µg/mL in PBS for 15min at RT while rocking. Fibers were then permeabilized in -20oC methanol for 5min, then blocked for 1 hour at RT with blocking solution (2% BSA, 0.4% Triton X-100 in PBS), followed by the application of primary antibodies diluted in blocking solution; NFH (1:500; ab72996, Abcam) and CRMP4 (1:250; Millipore, AB5454) and incubation overnight at RT while rocking. On the next day, samples were incubated with species-specific fluorescent secondary antibodies for 4 hours at room temperature while rocking. Muscle fibers were then placed on a cover slide suitable for imaging, mounted with Vectashield (Vector Laboratories) and sealed with clear nail polish. Slides were kept in RT until completely dried, then stored at 4oC until imaged in the microscope.

Proximity ligation assay

The proximity ligation assay (PLA) was used to visualize the co-localization of selected proteins; it was performed as previously described (Söderberg *et al*, 2008). Briefly, iPSc-derived MNs and murine-MN cultures were grown in the MFC on glass dishes for 18 and 5 DIV, respectively, and were then fixed in 4% PFA, at 4˚C for 20 minutes. Subsequently, the samples were blocked and permeabilized with 5% Donkey Serum, 1% BSA, and 0.1% Triton X-100 in PBS for 1h and incubated with anti-CRMP4 and anti-DIC antibodies overnight at 4˚C. Interactions (range ~40nm) were detected by the proximity ligation assay Duolink kit (Sigma: PLA probe anti-mouse minus DUO92004, anti-rabbit plus DUO92002, and the detection kit Far Red). PLA was performed according to the manufacturer's instructions. Coverslips were washed, mounted, and imaged by confocal microscopy. Half ligation samples were used as a negative control. The axonal PLA signal was quantified with ImageJ software using an axonal mask based on an endogenous mCherry/Rosa signal. The PLA puncta signal was quantified with the analyzed particle function of the software.

CRMP4-like Peptide design and insertion into MNs

The Dynein-CRMP4 blocking peptide design was based on previous findings by Amrimura et al., which pointed to 50 specific amino acid sequences responsible for

CRMP2 binding to dynein (Arimura *et al*, 2009). Peptides were prepared by Alomone labs and GL Biochem. Peptide sequences are as follows:

Name	Sequence	MW (Da)
Peptide-1	TTMIIDHVVPEPE	**1480 Da**
Peptide-2	SSLTEAYEKWREWADGKS	**2143 Da**
Peptide-3	CCDYALHVDI	**1151 Da**
Peptide-4	THWNDSVKQ	**1114 Da**

The peptides were inserted into axons by harsh pipetting. Final concentration of 10uM of each peptide were inserted. Tamra peptide was generously donated by Dr. Mike Fainzilber's lab (10uM final concentration).

Vectors

CRMP4 and CRMP4Δ100-150 (containing deletion of the coding sequence 301-450bp) were sub-cloned in frame into the pLL3.7-GFP (Addgene) mammalian expression vector. Flag-CRMP4 and mutated Flag-CRMP4-I141V, used in the pull-down assays, was cloned into pCDNA3 vector (Invitrogen). GFP and GFP-50aa (containing the coding sequence of CRMP4 301-450bp) were sub-cloned in frame into the pAAV-CBh (Vector Builder) mammalian gene expression vector.

Experimental design and statistical analysis

All statistical analyses were performed using GraphPad Prism v6.0. For two-group analysis, Student's t-test or the Mann-Whitney test was used, as determined by a normality test. For multiple comparisons, Anova was used with the Tukey or Holm-Sidak post-hoc tests. All experiments include at least 3 biologically independent repeats, Significance was set at $p<0.05$.

Data Availability

This study includes no data deposited in external repositories. All data generated or analyzed during this study are included in this published article.

Acknowledgments

This work was supported by IsrALS Foundation, the Israel Science Foundation (735/19), and the European Research Council (grant number 309377) to E.P, Czech Health Research Council grant no. NV18-04-00085 to MB, Czech Science Foundation grant no. 21-24571S to MB and RW, and Grant Agency of the Charles

University grants no. 524218 to RW. We thank Prof. Mike Fainzilber for the Tamra peptides, and help in AAV9. We thank Prof. Eva Feldman and Prof. Stephen Goutman for obtaining the fibroblasts for the IPSC lines. We thank Dr. Michael Tolmasov for performing the intrathecal injections. We thanks Michigan Brain Bank (5P30 AG053760 University of Michigan Alzheimer's Disease Core Center) for providing patients spinal cord sections. Immunohistochemistry (IHC) was performed at the Rogel Cancer Center Tissue and Molecular Pathology Shared Resource Laboratory (funding support: NIH P30 CA04659229).

Abbreviations

ALS - Amyotrophic Lateral Sclerosis
BDNF - Brain-Derived Neurotrophic Factor
CNTF - Ciliary Neurotrophic Factor
CTX – Alexa Fluor 647-conjugated Cholera toxin subunit B
C9orf72 - Chromosome 9 open reading frame 72
CRMPs – Collapsin Respond Mediator Proteins
DIV - Days In Vitro
Dyn-In - Ciliobrevin-D (Dynein Inhibitor)
GFP-CRMP4Δ100-150
GDNF - Glial-Derived Neurotrophic
IPSC – Induced Pluripotent Stem Cells
JNK - c-Jun N-terminal kinases
MFC - Microfluidic Chambers
MNs - Motor Neurons
NMJ - Neuromuscular Junction
NRP1 - Neuropilin 1
PTEN - Phosphatase and tensin homolog
PLO - Poly D-L-ornithine
PLA - Proximity Ligation Assay
PDMS - Polydimethylsiloxane
PNB - Poor Neuorobasal medium (neurotrophin- and serum-free medium)
SOD1 - Cu/Zn Superoxide Dismutase 1
Sema3A - Semaphorin3A
SN – Sciatic Nervep75^{NTR} - low-affinity nerve growth factor receptor

Ethics approval and consent to participate

Animal experiments were performed under the supervision and approval of the Tel-Aviv University Committee for Animal Ethics. Human iPSC experiments were performed under the supervision and approval of the Tel-Aviv University Committee for Human Ethics.

Conflict of Interest

The authors declare that they have no conflict of interest point.

Author Contribution

Project conceptualization by RM, LA, TGP, MB, and EP; Data curation by RM, LA, TGP, TA, AI; Formal analysis by RM, LA, TGP, AI, MO, EP; Investigation by RM, LA, TGP, TA, RW, MO, ET, GA, NS, AD, SB; Methodology by RM, LA, TGP, TA, AI, RW, MO, ET, GA, NS, YA, AD, SB, MB, EP; Resource obtain from ET, GA, NS, AD,SB; Funding acquisition MB, EP; Supervision MB, EP; Writing—original draft, review and editing by RM, LA, TGP, TA, AI, YA, AD, SB, MB, EP and approved by all.

References:

Arimura N, Hattori A, Kimura T, Nakamuta S, Funahashi Y, Hirotsune S, Furuta K, Urano T, Toyoshima YY & Kaibuchi K (2009) CRMP-2 directly binds to cytoplasmic dynein and interferes with its activity. *J Neurochem* 111: 380–390

Balastik M, Zhou XZ, Alberich-Jorda M, Weissova R, Žiak J, Pazyra-Murphy MF, Cosker KE, Machonova O, Kozmikova I, Chen C-H, *et al* (2015) Prolyl Isomerase Pin1 Regulates Axon Guidance by Stabilizing CRMP2A Selectively in Distal Axons. *Cell Rep* 13: 812–828

Bamji SX, Majdan M, Pozniak CD, Belliveau DJ, Aloyz R, Kohn J, Causing CG & Miller FD (1998) The p75 neurotrophin receptor mediates neuronal apoptosis and is essential for naturally occurring sympathetic neuron death. *J Cell Biol* 140: 911–23

Ben-Zvi A, Ben-Gigi L, Klein H & Behar O (2007) Modulation of semaphorin3A activity by p75 neurotrophin receptor influences peripheral axon patterning. *J Neurosci* 27: 13000–11

Bilsland LG, Sahai E, Kelly G, Golding M, Greensmith L & Schiavo G (2010) Deficits in axonal transport precede ALS symptoms in vivo. *Proc Natl Acad Sci U S A* 107: 20523–8

Blasco H, Bernard-Marissal N, Vourc'h P, Guettard YO, Sunyach C, Augereau O,

Khederchah J, Mouzat K, Antar C, Gordon PH, *et al* (2013) A Rare Motor Neuron Deleterious Missense Mutation in the *DPYSL3* (*CRMP4*) Gene is Associated with ALS. *Hum Mutat* 34: 953–960

Boillée S, Vande Velde C & Cleveland DW (2006) ALS: A Disease of Motor Neurons and Their Nonneuronal Neighbors. *Neuron* 52: 39–59

Cagnetta R, Frese CK, Shigeoka T, Krijgsveld J & Holt CE (2018) Rapid Cue-Specific Remodeling of the Nascent Axonal Proteome. *Neuron* 99: 29-46.e4

Cagnetta R, Wong HH-W, Frese CK, Mallucci GR, Krijgsveld J & Holt CE (2019) Noncanonical Modulation of the eIF2 Pathway Controls an Increase in Local Translation during Neural Wiring. *Mol Cell* 73: 474-489.e5

Campbell DS & Holt CE (2001) Chemotropic responses of retinal growth cones mediated by rapid local protein synthesis and degradation. *Neuron* 32: 1013–26

de Carvalho M, Dengler R, Eisen A, England JD, Kaji R, Kimura J, Mills K, Mitsumoto H, Nodera H, Shefner J, *et al* (2008) Electrodiagnostic criteria for diagnosis of ALS. *Clin Neurophysiol* 119: 497–503 doi:10.1016/j.clinph.2007.09.143 [PREPRINT]

Castellani V, Falk J & Rougon G (2004) Semaphorin3A-induced receptor endocytosis during axon guidance responses is mediated by L1 CAM. *Mol Cell Neurosci* 26: 89–100

Chadborn NH, Ahmed AI, Holt MR, Prinjha R, Dunn GA, Jones GE & Eickholt BJ (2006) PTEN couples Sema3A signalling to growth cone collapse. *J Cell Sci* 119: 951–7

Charrier E, Reibel S, Rogemond V, Aguera M, Thomasset N & Honnorat J (2003) Collapsin Response Mediator Proteins (CRMPs): Involvement in Nervous System Development and Adult Neurodegenerative Disorders. *Mol Neurobiol* 28: 51–64

Cosker KE & Segal RA (2014) Neuronal signaling through endocytosis. *Cold Spring Harb Perspect Biol* 6

Costa CJ & Willis DE (2018) To the end of the line: Axonal mRNA transport and local translation in health and neurodegenerative disease. *Dev Neurobiol* 78: 209–220

Deinhardt K, Salinas S, Verastegui C, Watson R, Worth D, Hanrahan S, Bucci C & Schiavo G (2006) Rab5 and Rab7 Control Endocytic Sorting along the Axonal Retrograde Transport Pathway. *Neuron* 52: 293–305

DeJesus-Hernandez M, Mackenzie IR, Boeve BF, Boxer AL, Baker M, Rutherford NJ, Nicholson AM, Finch NA, Flynn H, Adamson J, *et al* (2011) Expanded GGGGCC Hexanucleotide Repeat in Noncoding Region of C9ORF72 Causes

899 Chromosome 9p-Linked FTD and ALS. *Neuron* 72: 245–256
900 Duplan L, Bernard N, Casseron W, Dudley K, Thouvenot E, Honnorat J, Rogemond
901 V, De Bovis B, Aebischer P, Marin P, *et al* (2010) Collapsin response mediator
902 protein 4a (CRMP4a) is upregulated in motoneurons of mutant SOD1 mice and
903 can trigger motoneuron axonal degeneration and cell death. *J Neurosci* 30:
904 785–96
905 Escudero CA, Cabeza C, Moya-Alvarado G, Maloney MT, Flores CM, Wu C, Court
906 FA, Mobley WC & Bronfman FC (2019) c-Jun N-terminal kinase (JNK)-
907 dependent internalization and Rab5-dependent endocytic sorting mediate long-
908 distance retrograde neuronal death induced by axonal BDNF-p75 signaling. *Sci*
909 *Rep* 9: 6070
910 Firestone AJ, Weinger JS, Maldonado M, Barlan K, Langston LD, O'Donnell M,
911 Gelfand VI, Kapoor TM & Chen JK (2012) Small-molecule inhibitors of the AAA+
912 ATPase motor cytoplasmic dynein. *Nature* 484: 125–9
913 Fischer LR, Culver DG, Tennant P, Davis AA, Wang M, Castellano-Sanchez A, Khan
914 J, Polak MA & Glass JD (2004) Amyotrophic lateral sclerosis is a distal
915 axonopathy: evidence in mice and man. *Exp Neurol* 185: 232–40
916 Fournier AE, Nakamura F, Kawamoto S, Goshima Y, Kalb RG & Strittmatter SM
917 (2000) Semaphorin3a Enhances Endocytosis at Sites of Receptor–F-Actin
918 Colocalization during Growth Cone Collapse. *J Cell Biol* 149: 411–422
919 Frey D, Schneider C, Xu L, Borg J, Spooren W & Caroni P (2000) Early and selective
920 loss of neuromuscular synapse subtypes with low sprouting competence in
921 motoneuron diseases. *J Neurosci* 20: 2534–42
922 Gershoni-Emek N, Chein M, Gluska S & Perlson E (2015) Amyotrophic Lateral
923 Sclerosis as a Spatiotemporal Mislocalization Disease: Location, Location,
924 Location. *Int Rev Cell Mol Biol* 315: 23–71
925 Ghosh AS, Wang B, Pozniak CD, Chen M, Watts RJ & Lewcock JW (2011) DLK
926 induces developmental neuronal degeneration via selective regulation of
927 proapoptotic JNK activity. *J Cell Biol* 194: 751–764
928 Gibbs KL, Kalmar B, Rhymes ER, Fellows AD, Ahmed M, Whiting P, Davies CH,
929 Greensmith L & Schiavo G (2018) Inhibiting p38 MAPK alpha rescues axonal
930 retrograde transport defects in a mouse model of ALS. *Cell Death Dis* 9: 596
931 Goshima Y, Nakamura F, Strittmatter P & Strittmatter SM (1995) Collapsin-induced
932 growth cone collapse mediated by an intracellular protein related to UNC-33.
933 *Nature*
934 Guedes-Dias P & Holzbaur ELF (2019) Axonal transport: Driving synaptic function.
935 *Science (80-)* doi:10.1126/science.aaw9997 [PREPRINT]

Haramati S, Chapnik E, Sztainberg Y, Eilam R, Zwang R, Gershoni N, McGlinn E, Heiser PW, Wills A-M, Wirguin I, *et al* (2010) miRNA malfunction causes spinal motor neuron disease. *Proc Natl Acad Sci U S A* 107: 13111–6

Harrington AW & Ginty DD (2013) Long-distance retrograde neurotrophic factor signalling in neurons. *Nat Rev Neurosci* 14: 177–87

Howard J, Hudspeth AJ & Vale RD (1989) Movement of microtubules by single kinesin molecules. *Nature* 342: 154–158

Ionescu A, Zahavi EE, Gradus T, Ben-Yaakov K & Perlson E (2016) Compartmental microfluidic system for studying muscle–neuron communication and neuromuscular junction maintenance. *Eur J Cell Biol* 95: 69–88

Jang SY, Shin YK, Jung J, Lee SH, Seo SY, Suh DJ & Park HT (2010) Injury-induced CRMP4 expression in adult sensory neurons; a possible target gene for ciliary neurotrophic factor. *Neurosci Lett* 485: 37–42

Kenchappa RS, Tep C, Korade Z, Urra S, Bronfman FC, Yoon SO & Carter BD (2010) p75 neurotrophin receptor-mediated apoptosis in sympathetic neurons involves a biphasic activation of JNK and up-regulation of tumor necrosis factor-alpha-converting enzyme/ADAM17. *J Biol Chem* 285: 20358–68

LaMonte BH, Wallace KE, Holloway BA, Shelly SS, Ascaño J, Tokito M, Van Winkle T, Howland DS & Holzbaur ELF (2002) Disruption of dynein/dynactin inhibits axonal transport in motor neurons causing late-onset progressive degeneration. *Neuron* 34: 715–27

Macia E, Ehrlich M, Massol R, Boucrot E, Brunner C & Kirchhausen T (2006) Dynasore, a cell-permeable inhibitor of dynamin. *Dev Cell* 10: 839–50

Maimon R, Ionescu A, Bonnie A, Sweetat S, Wald-Altman S, Inbar S, Gradus T, Trotti D, Weil M, Behar O, *et al* (2018) miR126-5p Downregulation Facilitates Axon Degeneration and NMJ Disruption via a Non-Cell-Autonomous Mechanism in ALS. *J Neurosci* 38: 5478–5494

Manns RPC, Cook GMW, Holt CE & Keynes RJ (2012) Differing semaphorin 3A concentrations trigger distinct signaling mechanisms in growth cone collapse. *J Neurosci* 32: 8554–9

Millecamps S & Julien J-P (2013) Axonal transport deficits and neurodegenerative diseases. *Nat Rev Neurosci* 14: 161–176

Moloney EB, de Winter F & Verhaagen J (2014) ALS as a distal axonopathy: molecular mechanisms affecting neuromuscular junction stability in the presymptomatic stages of the disease. *Front Neurosci* 8: 252

Münch C, Sedlmeier R, Meyer T, Homberg V, Sperfeld AD, Kurt A, Prudlo J, Peraus G, Hanemann CO, Stumm G, *et al* (2004) Point mutations of the p150 subunit of

973 dynactin (DCTN1) gene in ALS. *Neurology* 63: 724–6
974 Nagai J, Baba R & Ohshima T (2017) CRMPs Function in Neurons and Glial Cells:
975 Potential Therapeutic Targets for Neurodegenerative Diseases and CNS Injury.
976 *Mol Neurobiol* 54: 4243–4256
977 Nagai J, Kitamura Y, Owada K, Yamashita N, Takei K, Goshima Y & Ohshima T
978 (2015) Crmp4 deletion promotes recovery from spinal cord injury by
979 neuroprotection and limited scar formation. *Sci Rep* 5: 8269
980 Nicolas A, Kenna KP, Renton AE, Ticozzi N, Faghri F, Chia R, Dominov JA, Kenna
981 BJ, Nalls MA, Keagle P, *et al* (2018) Genome-wide Analyses Identify KIF5A as a
982 Novel ALS Gene. *Neuron* 97: 1268-1283.e6
983 Olenick MA, Dominguez R & Holzbaur ELF (2019) Dynein activator Hook1 is
984 required for trafficking of BDNF-signaling endosomes in neurons. *J Cell Biol*
985 218: 220–233
986 Paschal BM & Vallee RB (1987) Retrograde transport by the microtubule-associated
987 protein MAP 1C. *Nature* 330: 181–183
988 Pasinelli P, Borchelt DR, Houseweart MK, Cleveland DW & Brown RH (1998)
989 Caspase-1 is activated in neural cells and tissue with amyotrophic lateral
990 sclerosis-associated mutations in copper-zinc superoxide dismutase. *Proc Natl*
991 *Acad Sci U S A* 95: 15763–15768
992 Pathak A, Stanley EM, Hickman FE, Wallace N, Brewer B, Li D, Gluska S, Perlson E,
993 Fuhrmann S, Akassoglou K, *et al* (2018) Retrograde Degenerative Signaling
994 Mediated by the p75 Neurotrophin Receptor Requires p150Glued Deacetylation
995 by Axonal HDAC1. *Dev Cell* 46: 376-387.e7
996 Perlson E, Jeong G-B, Ross JL, Dixit R, Wallace KE, Kalb RG & Holzbaur ELF
997 (2009) A switch in retrograde signaling from survival to stress in rapid-onset
998 neurodegeneration. *J Neurosci* 29: 9903–17
999 Perlson E, Maday S, Fu M-M, Moughamian AJ & Holzbaur ELF (2010) Retrograde
1000 axonal transport: pathways to cell death? *Trends Neurosci* 33: 335–44
1001 Peters OM, Ghasemi M & Brown RH (2015) Emerging mechanisms of molecular
1002 pathology in ALS. *J Clin Invest* 125: 1767–79
1003 Ponnusamy R, Lebedev A, Pahlow S & Lohkamp B (2014) Crystal Structure of
1004 Human Crmp-4: Correction of Intensities for Lattice-Translocation Disorder. *Acta*
1005 *Crystallogr,SectD* 70: 1680
1006 Porter AG (1999) Protein translocation in apoptosis. *Trends Cell Biol* 9: 394–401
1007 doi:10.1016/S0962-8924(99)01624-4 [PREPRINT]
1008 Rahajeng J, Giridharan SSP, Naslavsky N & Caplan S (2010) Collapsin Response
1009 Mediator Protein-2 (Crmp2) Regulates Trafficking by Linking Endocytic

1010 Regulatory Proteins to Dynein Motors. *J Biol Chem* 285: 31918–31922
1011 Renton AE, Majounie E, Waite A, Simón-Sánchez J, Rollinson S, Gibbs JR,
1012 Schymick JC, Laaksovirta H, van Swieten JC, Myllykangas L, *et al* (2011) A
1013 Hexanucleotide Repeat Expansion in C9ORF72 Is the Cause of Chromosome
1014 9p21-Linked ALS-FTD. *Neuron* 72: 257–268
1015 Reyes NA, Fisher JK, Austgen K, VandenBerg S, Huang EJ & Oakes SA (2010)
1016 Blocking the mitochondrial apoptotic pathway preserves motor neuron viability
1017 and function in a mouse model of amyotrophic lateral sclerosis. *J Clin Invest*
1018 120: 3673–3679
1019 Rosen DR, Siddique T, Patterson D, Figlewicz DA, Sapp P, Hentati A, Donaldson D,
1020 Goto J, O'Regan JP, Deng H-X, *et al* (1993) Mutations in Cu/Zn superoxide
1021 dismutase gene are associated with familial amyotrophic lateral sclerosis.
1022 *Nature* 362: 59–62
1023 Rotem N, Magen I, Ionescu A, Gershoni-Emek N, Altman T, Costa CJ, Gradus T,
1024 Pasmanik-Chor M, Willis DE, Ben-Dov IZ, *et al* (2017) ALS Along the Axons –
1025 Expression of Coding and Noncoding RNA Differs in Axons of ALS models. *Sci*
1026 *Rep* 7: 44500
1027 Sasaki Y, Cheng C, Uchida Y, Nakajima O, Ohshima T, Yagi T, Taniguchi M,
1028 Nakayama T, Kishida R, Kudo Y, *et al* (2002) Fyn and Cdk5 Mediate
1029 Semaphorin-3A Signaling, Which Is Involved in Regulation of Dendrite
1030 Orientation in Cerebral Cortex. *Neuron* 35: 907–920
1031 Schmidt EF & Strittmatter SM (2007) The CRMP Family of Proteins and Their Role in
1032 Sema3A Signaling. In *Semaphorins: Receptor and Intracellular Signaling*
1033 *Mechanisms* pp 1–11. New York, NY: Springer New York
1034 Singh KK, Park KJ, Hong EJ, Kramer BM, Greenberg ME, Kaplan DR & Miller FD
1035 (2008) Developmental axon pruning mediated by BDNF-p75NTR-dependent
1036 axon degeneration. *Nat Neurosci* 11: 649–58
1037 Siu M, Sengupta Ghosh A & Lewcock JW (2018) Dual Leucine Zipper Kinase
1038 Inhibitors for the Treatment of Neurodegeneration. *J Med Chem* 61: 8078–8087
1039 doi:10.1021/acs.jmedchem.8b00370 [PREPRINT]
1040 Söderberg O, Leuchowius K-J, Gullberg M, Jarvius M, Weibrecht I, Larsson L-G &
1041 Landegren U (2008) Characterizing proteins and their interactions in cells and
1042 tissues using the in situ proximity ligation assay. *Methods* 45: 227–232
1043 Song W, Volosin M, Cragnolini AB, Hempstead BL & Friedman WJ (2010) ProNGF
1044 induces PTEN via p75NTR to suppress Trk-mediated survival signaling in brain
1045 neurons. *J Neurosci* 30: 15608–15
1046 Steinberg KM, Yu B, Koboldt DC, Mardis ER & Pamphlett R (2015) Exome

sequencing of case-unaffected-parents trios reveals recessive and de novo genetic variants in sporadic ALS. *Sci Rep* 5: 9124

Tank EM, Figueroa-Romero C, Hinder LM, Bedi K, Archbold HC, Li X, Weskamp K, Safren N, Paez-Colasante X, Pacut C, *et al* (2018) Abnormal RNA stability in amyotrophic lateral sclerosis. *Nat Commun* 9: 2845

Terenzio M, Schiavo G & Fainzilber M (2017) Compartmentalized Signaling in Neurons: From Cell Biology to Neuroscience. *Neuron* 96: 667–679

Valdez G, Tapia JC, Lichtman JW, Fox MA & Sanes JR (2012) Shared resistance to aging and ALS in neuromuscular junctions of specific muscles. *PLoS One* 7: e34640

De Vos KJ & Hafezparast M (2017) Neurobiology of axonal transport defects in motor neuron diseases: Opportunities for translational research? *Neurobiol Dis* 105: 283–299

Wu KY, Hengst U, Cox LJ, Macosko EZ, Jeromin A, Urquhart ER & Jaffrey SR (2005) Local translation of RhoA regulates growth cone collapse. *Nature* 436: 1020–1024

Yamashita N & Goshima Y (2012) Collapsin Response Mediator Proteins Regulate Neuronal Development and Plasticity by Switching Their Phosphorylation Status. *Mol Neurobiol* 45: 234–246

Zahavi EE, Ionescu A, Gluska S, Gradus T, Ben-Yaakov K & Perlson E (2015) A compartmentalized microfluidic neuromuscular co-culture system reveals spatial aspects of GDNF functions. *J Cell Sci* 128: 1241–52

Zahavi EE, Maimon R & Perlson E (2017) Spatial-specific functions in retrograde neuronal signalling. *Traffic*

Ziak J, Weissova R, Jeřábková K, Janikova M, Maimon R, Petrasek T, Pukajova B, Kleisnerova M, Wang M, Brill MS, *et al* (2020) CRMP 2 mediates Sema3F-dependent axon pruning and dendritic spine remodeling . *EMBO Rep*

Figure Legends

Figure 1 –CRMP4 is elevated in ALS diseased spinal cord neurons

(A, B) (A) Representative IHC images and (B) semi quantification of CRMP4 protein in human spinal cords (SC) cross sections from 2 control patients and 3 ALS patients. We analyzed total of 7 SC sections of controls and 14 SC sections of ALS patients, Data presented as mean ±SE. DAB: labeled CRMP4. Scale bar: left images 20 μm, right insets 10 μm. Mann-Whitney test ***p = 0.0003.

(C) Representative images of P90 SC cross sections of $SOD1^{G93A}$ and WT mice. Red: denotes NeuN, Green: denotes CRMP4. Scale bar: 10 μm.
(D) Quantification of the percentage of CRMP4 positive SC neurons in 3 WT VS. 3 $SOD1^{G93A}$ mice. We monitored CRMP4 expression in total of 108 cells in WT condition and 123 cells in $SOD1^{G93A}$, an average of 36 or 41 cells in each repeat respectively. Student's t-test, n = 3, Data presented as mean ±SE, *p = 0.0161.

Figure 2 –CRMP4 is mis localized in ALS motor units

(A) Representative images of ALS patient or non-ALS human control intra-muscular nerves. Red: denotes NFH, Green: denotes CRMP4, White: denotes co-localization area using Imaris software. Scale bar: 20 μm.
(B) Quantification of CRMP4 intensity levels in NFH positive intra-muscular distal nerves from 5 non-ALS controls and 4 sALS patients. We analyzed 40 terminal axons from the healthy samples (~8 axons per sample) and 36 terminal axons from sALS samples (~8 axons per sample). Data presented as mean ±SE. Student's t-test, *p = 0.0475.
(C) Representative images of $SOD1^{G93A/ChAT::tdTomato}$ or $WT^{ChAT::tdTomato}$ neuromuscular junctions at P90. White: denotes BTX, Red: denotes direct ChAT, Green: denotes CRMP4, Yellow: denotes Z projection of 3D Imaris co-localization of CRMP4 and ChAT. Scale bar: 10 μm.
(D) Quantification of CRMP4 positive NMJs in gastrocnemius muscles from 3 WT or 3 $SOD1^{G93A}$ P90 mice. Total of 44 NMJ's in WT condition and 60 NMJ's in $SOD1^{G93A}$ condition. Student's t-test, n=3, Data presented as mean ±SE, *p = 0.0157.
(E) Quantification of the percent of partially denervated NMJ's in the presence or absence of CRMP4 immunostaining in 3 different $SOD1^{G93A}$ mice. We counted 24 NMJ's in $SOD1^{G93A}$ CRMP4 negatives and 67 NMJ's in $SOD1^{G93A}$ CRMP4 positives. Student's t-test, n=3, Data presented as mean ±SE, *p = 0.0352.
(F) Representative images of P90 $SOD1^{G93A}$ and WT sciatic nerves. Red: denotes NFH, Blue: denotes GFAP and green denotes CRMP4, Yellow: denotes the Z projection of 3D Imaris co-localization of CRMP4 and NFH. Scale bar: 5 μm.
(G) Quantification of the co-localization area of CRMP4 with NFH in the sciatic nerve in 3 $SOD1^{G93A}$ mice compared to 3 WT mice using Imaris analysis. 14 WT sciatic nerve sections and 11 $SOD1^{G93A}$ sections were monitored. Data presented as mean ±SE. Student's t-test, n=3, ****p<0.0001.
(H-I) Western blot analysis and quantification of 3 independent repeats of P90 SN tissues for CRMP4 expression levels (size of ~64 KDa) in $SOD1^{G93A}$ compared to

1119 WT. tERK was used as a loading control (size of ~44 KDa). Student's t-test, n=3,
1120 Data presented as mean ±SE, *p = 0.0215.
1121
1122 **Figure 3 –CRMP4 protein levels are altered via a dynein-dependent activity**
1123 (A) Representative images of healthy or *C9orf72* iPSC-derived MNs treated with
1124 Sema3A or untreated in the distal compartment, 6 hours post treatment. Red:
1125 denotes Tubulin, Green: denotes CRMP4. Scale bar: 5 μm.
1126 (B) Quantification of CRMP4 intensity levels in healthy or *C9orf72* iPSC-derived MNs
1127 with Sema3A treatment or untreated. 14 untreated healthy axons, 12 healthy axons
1128 with Sema3A treatment, 49 untreated *C9orf72* axons and 31 *C9orf72* axons with
1129 Sema3A treatment were monitored from 3 different chambers. One-way ANOVA,
1130 Tukey's multiple comparisons test, n = 3, Data presented as mean ±SE, *p = 0.0338;
1131 ****p<0.0001.
1132 (C) Illustration of the experimental procedure for MNs in an MFC treated with the
1133 fluorescently tagged retrograde tracer CTX in the distal compartment. Neuronal cell
1134 bodies in the primary neuron whose axons have traversed into the distal
1135 compartment were also labeled by the retrograde tracer.
1136 (D) Representative images of healthy or C9orf72 human-derived MN cell somata with
1137 Sema3A treatment, Sema3A + dynein inhibitor treatment, or untreated. Gray:
1138 denotes CTX, Green: denotes CRMP4. Scale bar: 5μm.
1139 (E) Quantification of CRMP4 intensity (normalized to GAPDH+mCherry/area) levels
1140 at the somata of healthy or C9orf72 human-derived MN after Sema3A treatment,
1141 Sema3A + dynein inhibitor treatment, or untreated. Analysis performed in 3
1142 independent chambers per condition. 19 healthy untreated cell somata, 26 healthy
1143 cell somata with Sema3A treatment, 20 healthy cell somata with Sema3A + dynein
1144 inhibitor treatment and 14 *C9orf72* cell somata from each condition were monitored.
1145 One-way ANOVA, Newman-Keuls multiple comparisons test, n=3, Data presented as
1146 mean ±SE, *p=0.0207; ***p=0.0004.
1147 (F) Representative images of healthy or C9orf72 human-derived MN proximal axons
1148 with Sema3A treatment, Sema3A + dynein inhibitor treatment or untreated control.
1149 Green: denotes CRMP4, Red: denotes GAPDH. Scale bar: 5μm.
1150 (G) Quantification of CRMP4 intensity levels (normalized to GAPDH+mCherry/area)
1151 at the proximal axons in healthy or C9orf72 human-derived MN after Sema3A
1152 treatment, Sema3A + dynein inhibitor treatment, or untreated control. Analysis
1153 performed from 3 independent chambers in each condition. 21 healthy untreated
1154 proximal axons, 24 healthy proximal axons with Sema3A treatment, 16 healthy
1155 proximal axons with Sema3A + dynein inhibitor treatment, 12 *C9orf72* untreated

proximal axons, 8 *C9orf72* proximal axons with Sema3A treatment and 13 *C9orf72* proximal axons with Sema3A + dynein inhibitor treatment were monitored. One-way ANOVA, Newman-Keuls multiple comparisons test, n = 3, Data presented as mean ±SE, *p =0.0334, ****p<0.0001.

Figure 4 –CRMP4 binds dynein via a specific 50 amino acid motif

(A) Crystal structure (PDB code 4CNT) of a CRMP4 monomer (upper panel) and biological tetramer assembly (lower panel). The peptides that were selected to inhibit binding are highlighted and color coded as indicated.

(B) Upper panel represent the binding site domain of dynein in CRMP4 and its deletion. These constructs were used in the IP that was performed in the middle panel. Middle panel - Immunoprecipitation of DIC followed by western blot analysis of CRMP4 in COS7 cells overexpressing either GFP-CRMP4, or GFP-CRMP4 with deletion of amino acid 100-150, or GFP-CRMP4 overexpressing cells that were pre-incubated with a 10 µm mixture of peptides 1-4 (size of ~91 KDa). Lower panel - Western blot analysis of total protein levels before the pull-down assay (DIC size: ~75 KDa).

(C) Quantification of the Western blot in B from 3 independent repeats. The dynactin intensity band was normalized to the Flag-CRMP4 intensity band in each technical repeat. One-way ANOVA, Tukey's multiple comparisons test, n=3, Data presented as mean ±SE, **p=0.007, *p=0.0261.

(D) Upper panel - immunoprecipitation assay with anti-Flag antibody followed by Western blot analysis of dynactin (p150) in COS7 cells overexpressing Flag-CRMP4 (size of ~65 KDa). Lower panel - total protein input (size of ~150 KDa).

(E) Quantification of the blot in D from 3 independent repeats. The dynactin intensity band was normalized to the Flag-CRMP4 intensity band in each repeat. Student’s t-test, n=3, Data presented as mean ±SE, **p=0.01.

(F) Upper panel - Immunoprecipitation assay with anti-Flag antibody followed by Western blot analysis of dynactin (p150) in COS7 cells overexpressing Flag-CRMP4 (size of ~65 KDa). Lower panel - Total input (size of ~150 KDa).

(G) Quantification of the blot in F. The dynactin intensity band was normalized to the Flag-CRMP4 intensity band in each repeat. Student’s t-test, n=3, Data presented as mean ±SE, *p=0.0299.

(H) Immunoprecipitation of DIC (size of ~75 KDa) followed by Western blot analysis of CRMP4 (size of ~64 KDa) in COS7 cells that were transfected with CRMP4 and AAV9-50aa or its control. IgG antibody was used as a control.

(I) Quantification of the blot in H from 3 independent repeats. The CRMP4 intensity band was normalized to the DIC intensity band in each repeat. Student's t-test, n=3, Data presented as mean ±SE, *p=0.0479.

Figure 5 –CRMP4-dynein interaction is enhanced in ALS motor neuron axons

(A) Immunoprecipitation of DIC followed by Western blot analysis of CRMP4 in $SOD1^{G93A}$ compared to WT P90 sciatic nerves under physiological conditions. IgG antibody was used as a control.
(B) Quantification of the blot in A. 3 repeats, 12 sciatic nerves per condition were used in each repeat. The CRMP4 intensity band was normalized to the DIC intensity band in each repeat. Data presented as mean ±SE (Ratio Paired t-test, *p = 0.0416).
(C) Immunoprecipitation of DIC followed by Western blot analysis of CRMP4 in Cos7 cells that were transfected with mutant CRMP4 I141V compared to control. IgG antibody was used as a control.
(D) Quantification of four repeated pull down in C. The CRMP4 intensity band was normalized to the DIC intensity band for each repeat. (Student's t-test, n=4, Data presented as mean ±SE, *p=0.0393).
(E) Representative images from the proximity ligation assay (For explanation of PLA technique; please refer to method section) for CRMP4 and dynein in SOD^{G93A} and WT primary MNs axons that were exposed to either control or Sema3A 8h post treatment. Scale bar: 5µm.
(F) Quantification of the CRMP4-DIC puncta number per primary motor neuron axon in each condition. We analyzed ~20 axons per condition from 3 independent chambers per group (One-way ANOVA, Tukey's multiple comparisons test, n=3, Data presented as mean ±SE, **p=0.01 *p=0.04)
(G) Representative images of proximity ligation assay for CRMP4 and dynein in healthy and C9orf72 human-derived proximal axons post peptides treatment, Sema3A treatment, Sema3A + peptides treatment or untreated controls. Scale bar: 5µm.
(H) Quantification of the CRMP4-DIC puncta number per axon in healthy or C9orf72 human-derived MN proximal axons after Sema3A treatment, Sema3A + peptides treatment or untreated controls. Data collected from 3 independent chambers in each condition. Total of 37 healthy untreated proximal axons, 61 healthy proximal axons with peptides treatment, 59 healthy proximal axons with Sema3A treatment and 52 healthy proximal axons with Sema3A + peptides treatment. 67 *C9orf72* untreated

proximal axons, 63 *C9orf72* proximal axons with peptides treatment, 41 *C9orf72* proximal axons with Sema3A treatment and 50 *C9orf72* proximal axons with Sema3A + peptides treatment monitored. Data presented as mean ±SE. One-way ANOVA, Tukey's multiple comparisons test, n=3, ****p<0.0001.

Figure 6 – Retrograde CRMP4-dynein complex formation mediates MN loss in ALS

(A) Representative images of CTX signal in healthy and C9orf72 human IPSC-derived MNs before and after Sema3A application. Green: denotes CTX-positive cells. Yellow circles are numbered CTX positive cells. Purple circles are cells that are missing post Sema3A treatment. Scale bar: 40 μm.
(B-C) Quantification of CTX signal in healthy and C9orf72 IPSC-derived MNs before and 3 days after applying Sema3A to distal compartment, compared with untreated control. 3 independent chambers in each condition were analyzed. Average of ~150 neurons per condition monitored. Student's t-test, n=3, Data presented as mean ±SE, *p<0.05.
(D) Representative images of CTX signal in WT or $SOD1^{G93A}$ primary MNs before and 2 days after Sema3A application to the distal compartment in the presence of either Dynein inhibitor+Sema3A, Dynasore+Sema3A or untreated. Green: denotes CTX-positive cells. Yellow circles are numbered CTX positive cells. Purple circles are cells that are missing post Sema3A treatment. Scale bar: 30 μm.
(E) Quantification of CTX signal in a $SOD1^{G93A}$ explant before and 2 days after Sema3A application to the distal compartment in the presence of either Dynein inhibitor+Sema3A, Dynasore+Sema3A. 3 independent chambers in each condition were analyzed. ~200 neurons were monitored per each condition. One-way ANOVA, Tukey's multiple comparisons test, n = 3, Data presented as mean ±SE, *p<0.05, **p<0.01. Dynein inhibitor and Dynasore treatments were used as a negative control.
(F-G) Representative images and quantification of C9orf72 iPSC-derived MNs in the proximal compartment of an MFC before and after Sema3A treatment with and without 10 ug peptides 1-4. Green: denotes CTX-positive cells. Yellow circles are numbered CTX positive cells. Purple circles are cells that are missing post Sema3A treatment. 3 independent chambers in each condition were analyzed. ~200 neurons per condition monitored. Scale bar: 40μm. One-way ANOVA Tukey's multiple comparisons test, n = 3, Data presented as mean ±SE, **p =0.004.

Figure 7 – Blocking the formation of the CRMP4-dynein complexes reduces motor neuron toxicity *in vivo*

(A) Representative images and insets of P90 WT and SOD1^{G93A} SC cross sections at P90. Blue: denotes DAPI, Red: denoted NeuN, and White: denotes activated caspase 3. Scale bar: 20 μm.

(B) Quantification of active caspase 3 positive cells in P90 WT and SOD1^{G93A} SC. 3 different mice in each condition analyzed. We monitored active caspase 3 expression in total of 108 cells in WT SC and 123 cells in SOD1^{G93A}. Student's t-test, n=3, Data presented as mean ±SE, ****p<0.0001.

(C) Representative images of P90 SOD1^{G93A} mice SC cross sections that were injected with AAV9-GFP/AAV9-50aa-GFP. Blue: denotes DAPI, Red: denoted NeuN, and White: denotes activated caspase 3. Scale bar: 10 μm.

(D) Quantification of caspase 3 positive cells in P90 SOD1^{G93A} mice SC cross sections that were injected with either AAV9-GFP or AAV9-50aa-GFP. Data collected from 3 different mice in each condition. We monitored active caspase 3 expression in total of 228 cells in in P90 SOD1^{G93A} mice SC cross sections that were injected with AAV9-GFP and 179 cells P90 SOD1^{G93A} mice SC cross sections that were injected with AAV9-50aa-GFP. Student's t-test, n=3, Data presented as mean ±SE, ** p=0.0019.

(E) Quantification of the number of NeuN positive cells in P90 SOD1^{G93A} mice SC cross sections that were injected with either AAV9-GFP or AAV9-50aa-GFP. Data collected from 3 different mice in each condition. We monitored the number of NeuN positive cells from total of 228 cells in P90 SOD1^{G93A} mice SC cross sections that were injected with AAV9-GFP and 179 cells P90 SOD1^{G93A} mice SC cross sections that were injected with AAV9-50aa-GFP. Unpaired t test with Welch's correction, n=3, Data presented as mean ±SE, * p=0.0484.

(F) Working model – CRMP4-dynein complex formation is enhanced in ALS disease and leads to subtype-specific neuronal loss.

Figure 1

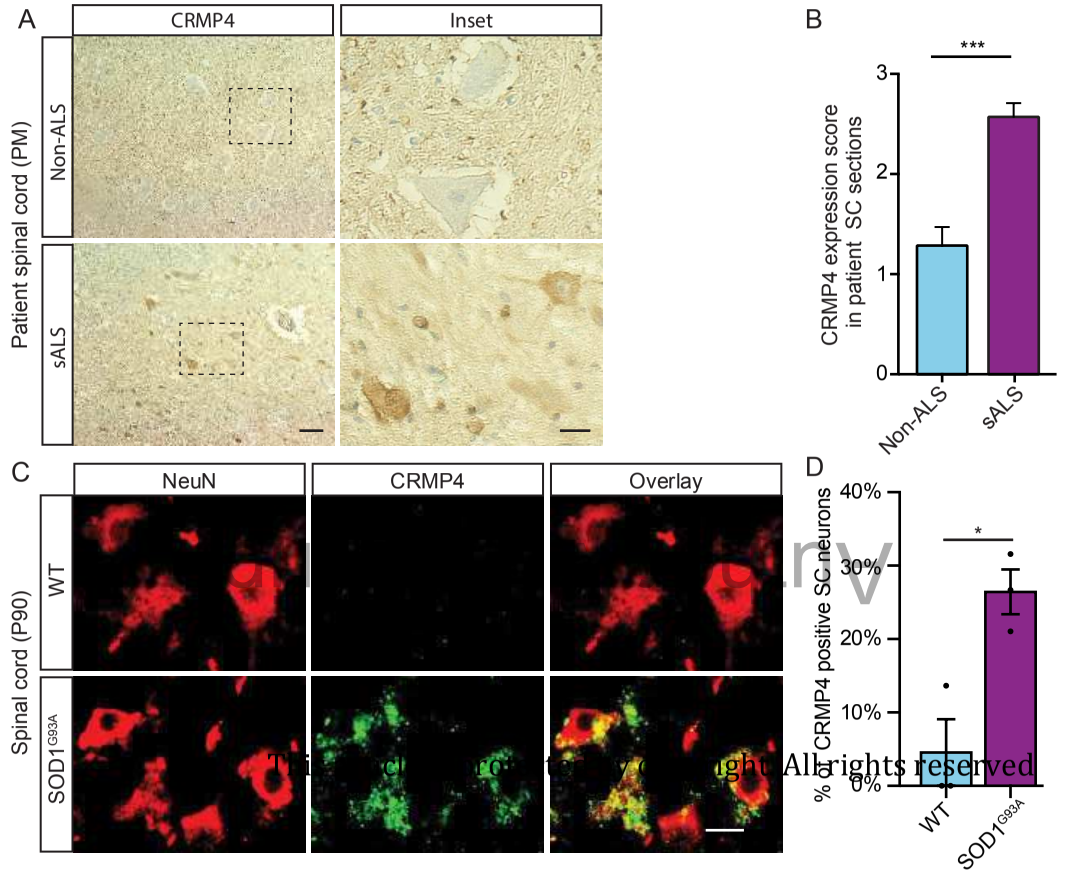

Figure 2

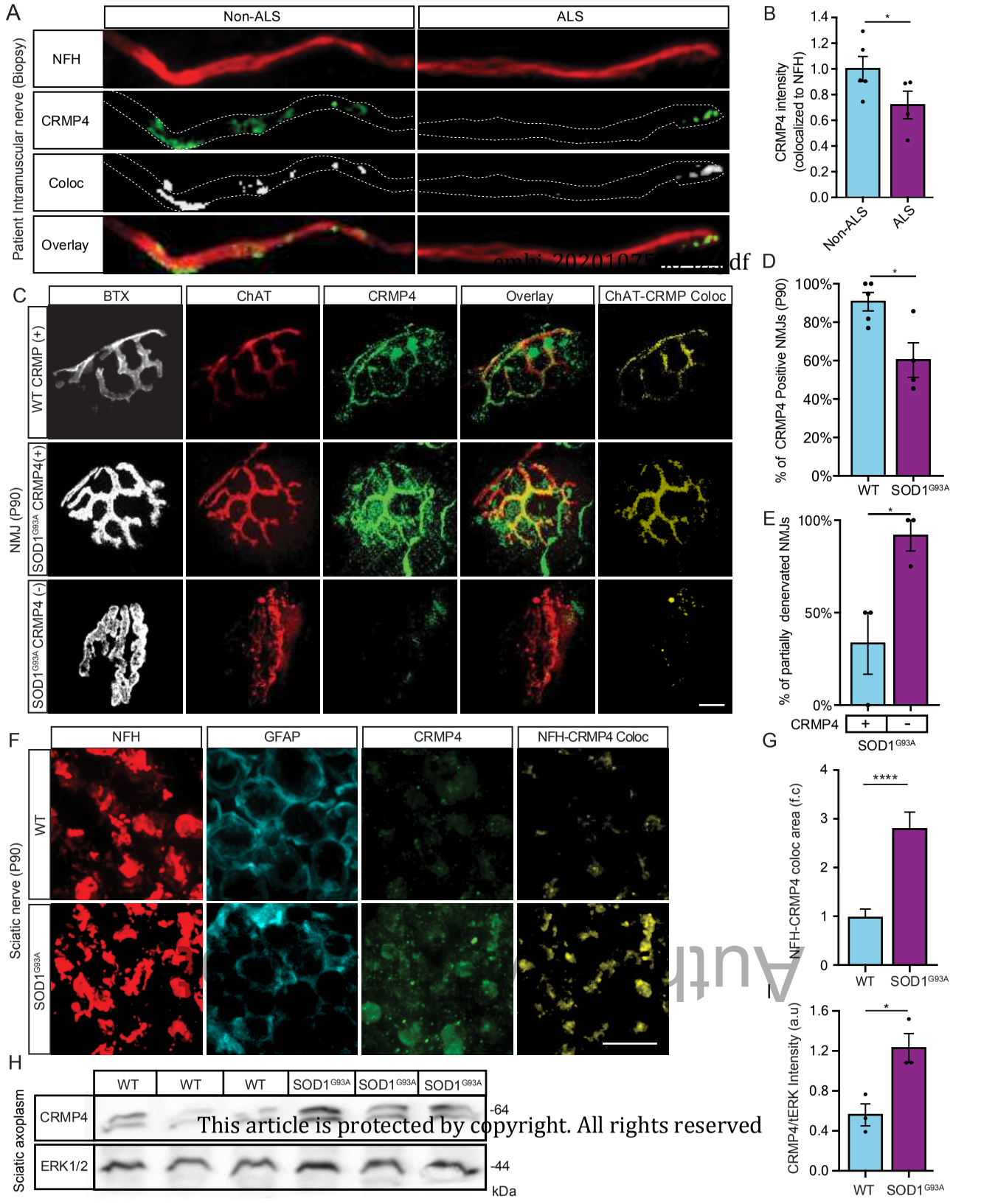

Figure 3

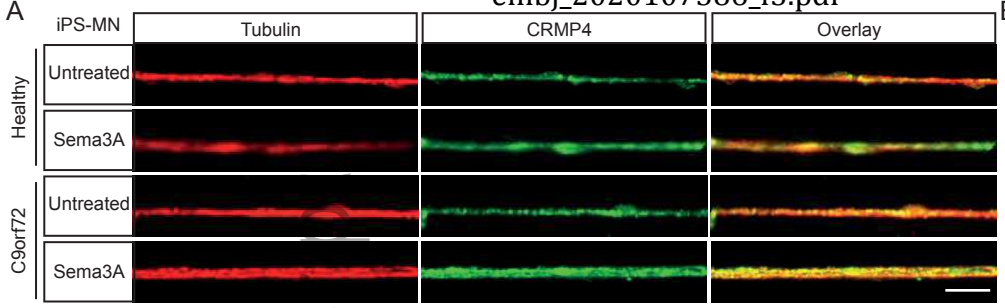

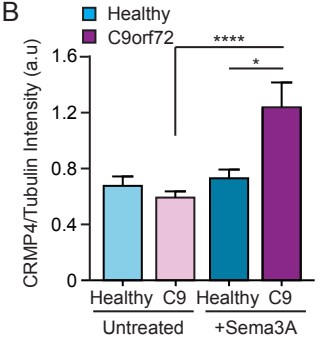

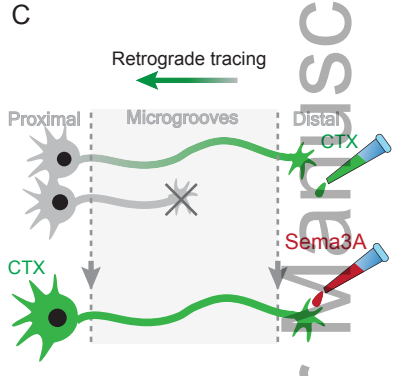

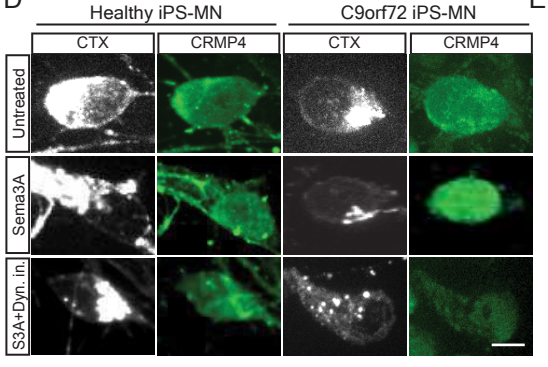

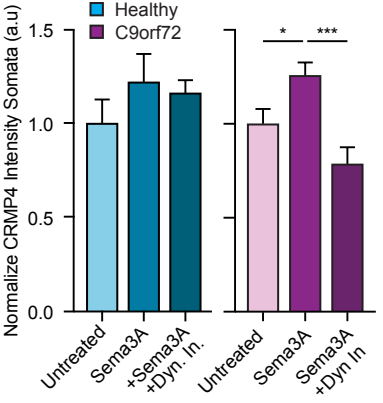

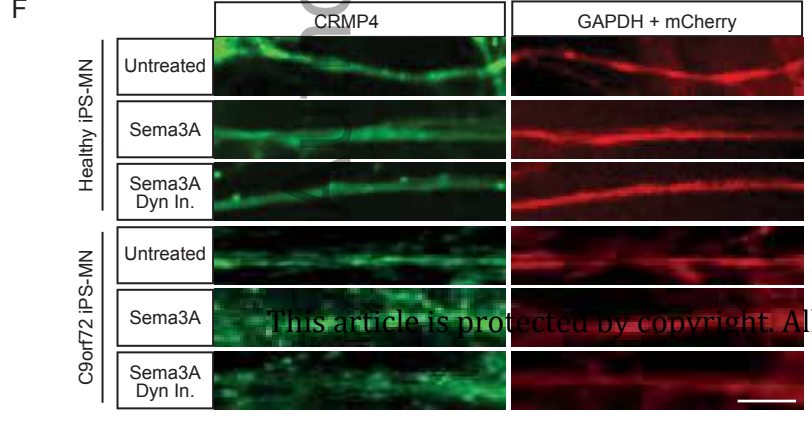

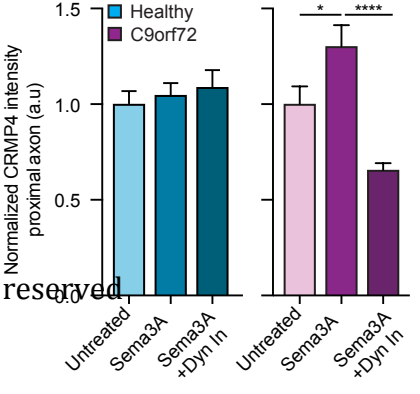

Figure 4

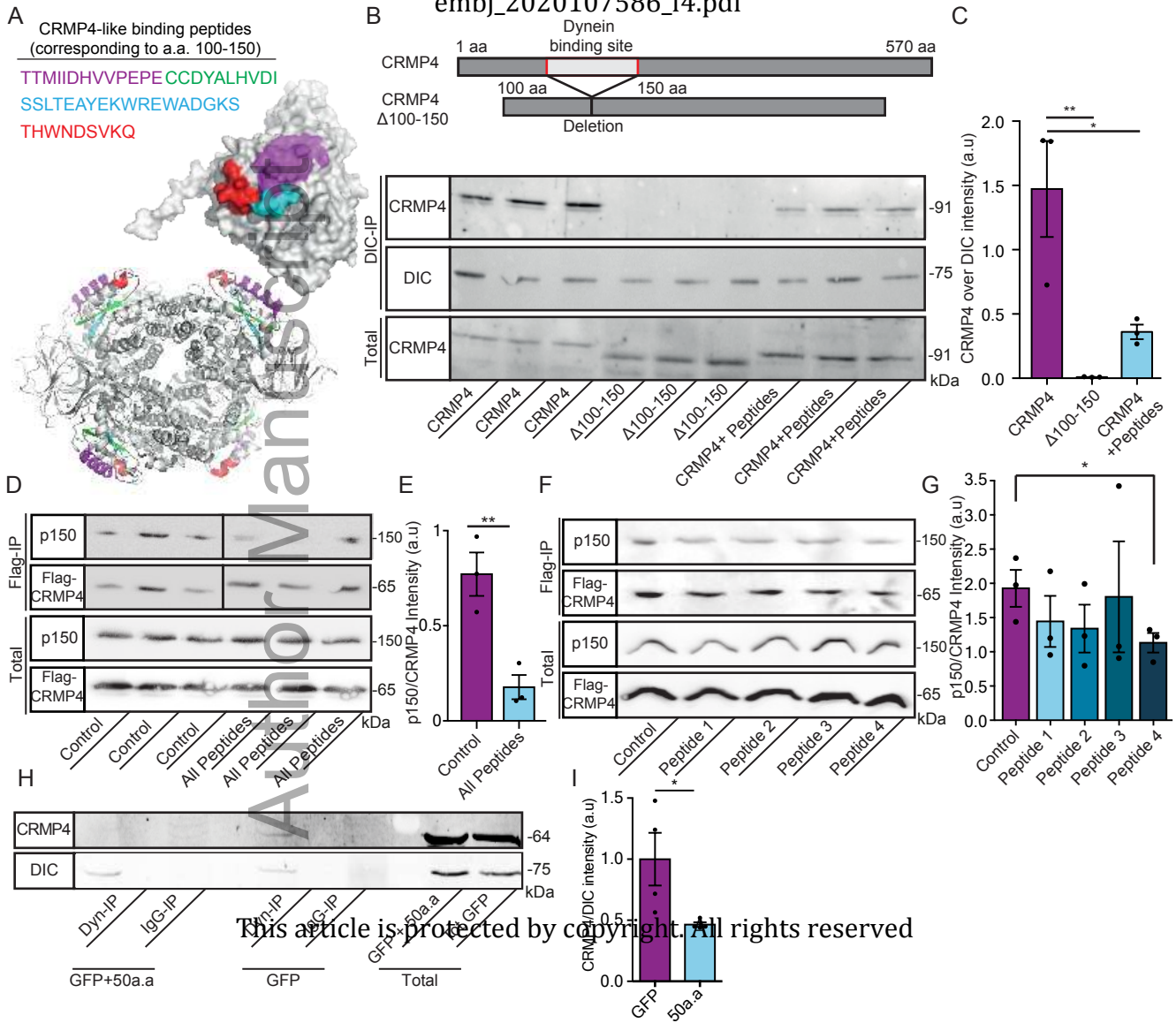

Figure 5

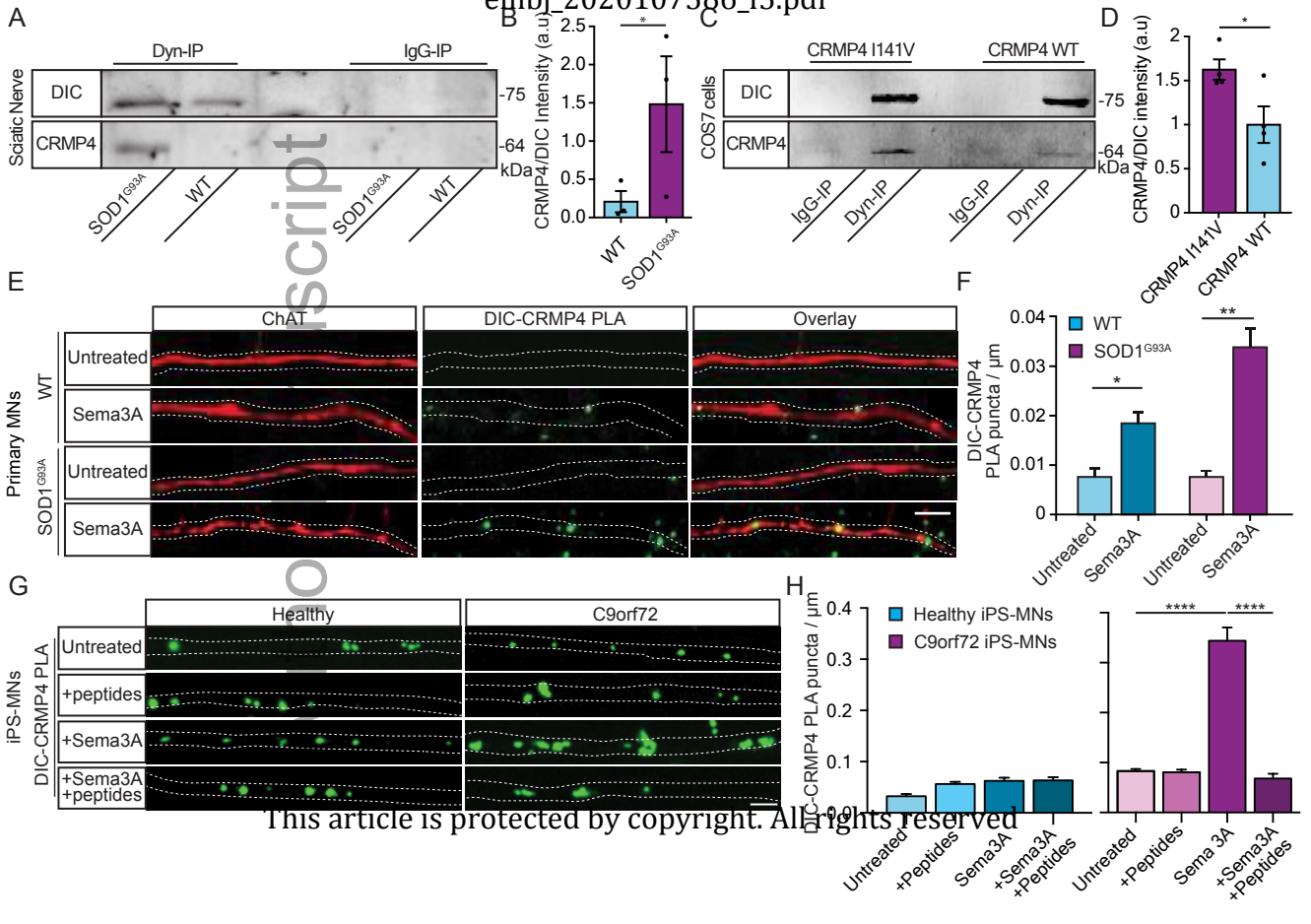

Figure 6

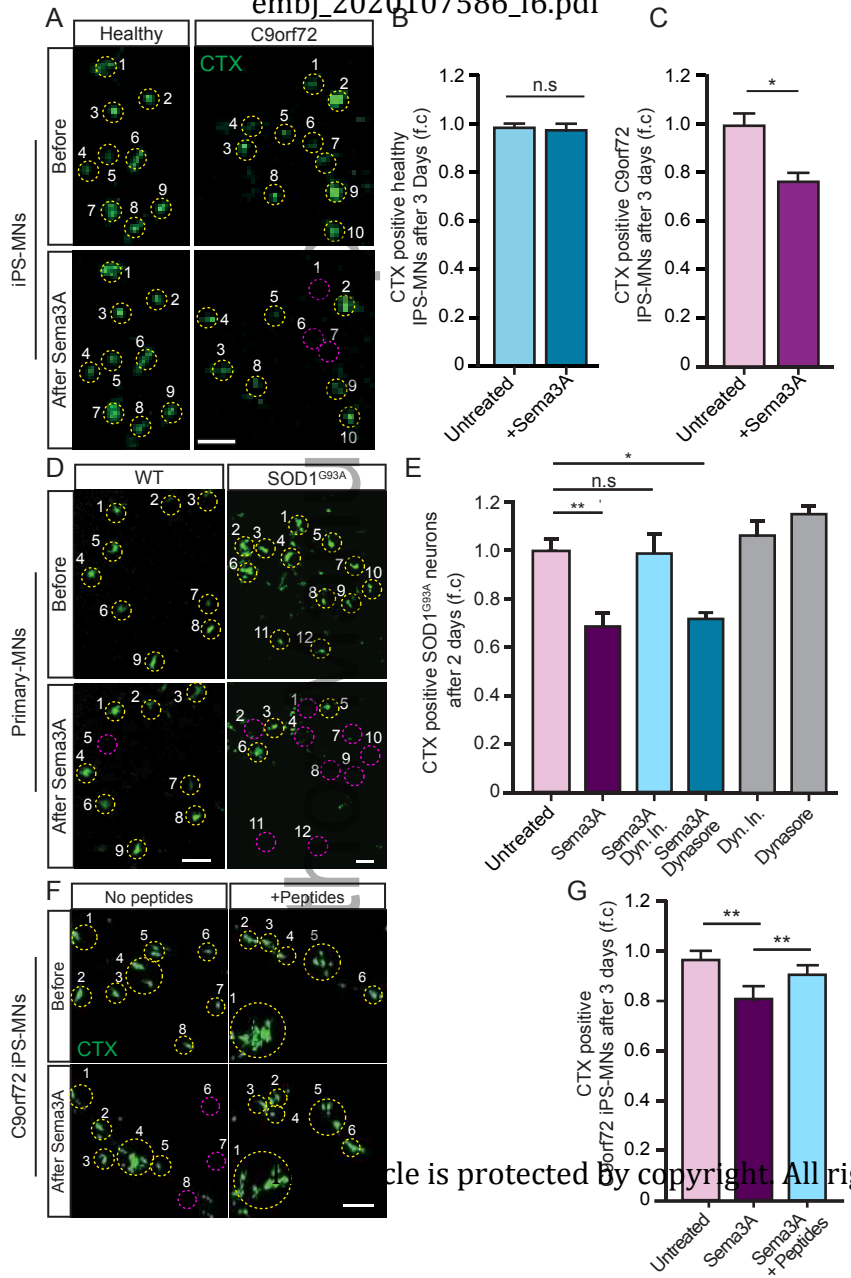

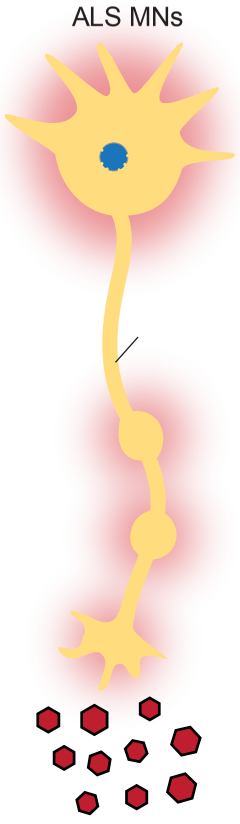
ALS MNs